J|A|C|S
ARTICLES
Published on Web 02/14/2002

Nickel(II)−Molybdenum(III)−Cyanide Clusters: Synthesis and Magnetic Behavior of Species Incorporating [(Me$_3$tacn)Mo(CN)$_3$]

Matthew P. Shores, Jennifer J. Sokol, and Jeffrey R. Long*

Contribution from the Department of Chemistry, University of California, Berkeley, California 94720-1460

Received July 6, 2001

Abstract: The substitution of Mo^{III} for Cr^{III} in metal−cyanide clusters is demonstrated as an effective means of increasing the strength of the magnetic exchange coupling and introducing magnetic anisotropy. Synthesis of the octahedral complex [(Me$_3$tacn)Mo(CN)$_3$] (Me$_3$tacn = *N*,*N*′,*N*″-trimethyl-1,4,7-triazacyclononane) is accomplished with the addition of precisely 3 equiv of LiCN to a solution of [(Me$_3$tacn)Mo(CF$_3$SO$_3$)$_3$] in DMF. An excess of LiCN prompts formation of a seven-coordinate complex, [(Me$_3$tacn)Mo(CN)$_4$]$^{1-}$, whereas less LiCN produces multinuclear species such as [(Me$_3$tacn)$_2$Mo$_2$(CN)$_5$]$^{1+}$. In close parallel to reactions previously performed with [(Me$_3$tacn)Cr(CN)$_3$], assembly reactions between [(Me$_3$tacn)Mo(CN)$_3$] and [Ni(H$_2$O)$_6$]$^{2+}$ or [(cyclam)Ni(H$_2$O)$_2$]$^{2+}$ (cyclam = 1,4,8,11-tetraazacyclotetradecane) afford face-centered cubic [(Me$_3$tacn)$_8$Mo$_8$Ni$_6$(CN)$_{24}$]$^{12+}$ and linear [(Me$_3$tacn)$_2$(cyclam)NiMo$_2$(CN)$_6$]$^{2+}$ clusters, respectively. Generation of the former involves a thermally induced cyanide linkage isomerization, which rapidly leads to a low-spin form of the cluster containing diamagnetic Ni^{II} centers. The cyclic voltammagram of this species in DMF reveals a sequence of six successive reduction waves spaced approximately 130 mV apart, suggesting class II mixed-valence behavior upon reduction. The magnetic properties of the aforementioned linear cluster are consistent with the expected ferromagnetic coupling and an $S = 4$ ground state, but otherwise vary slightly with the specific conformation adopted (as influenced by the packing of associated counteranions and solvate molecules in the crystal). Magnetization data indicate an axial zero-field splitting parameter with a magnitude falling in the range $|D| = 0.44-0.72$ cm^{-1}, and fits to the magnetic susceptibility data yield exchange coupling constants in the range $J = 17.0-17.6$ cm^{-1}. These values represent significant increases over those displayed by the analogous Cr^{III}-containing cluster. When perchlorate is used as a counteranion, [(Me$_3$tacn)$_2$(cyclam)NiMo$_2$(CN)$_6$]$^{2+}$ crystallizes from water in a dimeric form with pairs of the linear clusters directly linked via hydrogen bonding. In this case, fitting the magnetic susceptibility data requires use of two coupling constants: one intramolecular with $J = 14.9$ cm^{-1} and another intermolecular with $J' = -1.9$ cm^{-1}. Reacting [(Me$_3$tacn)Mo(CN)$_3$] with a large excess of [(cyclam)Ni(H$_2$O)$_2$]$^{2+}$ produces a [(Me$_3$tacn)$_2$(cyclam)$_3$(H$_2$O)$_2$Ni$_3$Mo$_2$(CN)$_6$]$^{6+}$ cluster possessing a zigzag structure that is a simple extension of the linear cluster geometry. Its magnetic behavior is consistent with weaker ferromagnetic coupling and an $S = 6$ ground state. Similar reactions employing an equimolar ratio of reactants afford related one-dimensional chains of formula [(Me$_3$tacn)(cyclam)NiMo(CN)$_3$]$^{2+}$. Once again, the ensuing structure depends on the associated counteranions, and the magnetic behavior indicates ferromagnetic coupling. It is hoped that substitutions of the type exemplified here will be of utility in the design of new single-molecule magnets.

Introduction

A decade ago, the molecular cluster [Mn$_{12}$O$_{12}$(CH$_3$CO$_2$)$_{16}$(H$_2$O)$_4$] was discovered to exhibit slow magnetic relaxation at low temperatures.[1] This unusual behavior is attributed to the presence of a high-spin ground state of $S = 10$, which, combined with an axial magnetic anisotropy of $D = -0.5$ cm^{-1}, leads to a spin reversal barrier of $S^2|D| = 50$ cm^{-1}.[1,2] The possibility of one day utilizing such "single-molecule magnets" for data storage applications has fueled a search for clusters with higher blocking temperatures.[3] However, of the dozen or so clusters now demonstrated to display a slow relaxation effect, none possess a spin reversal barrier greater than that of the Mn$_{12}$

(1) (a) Caneschi, A.; Gatteschi, D.; Sessoli, R.; Barra, A. L.; Brunel, L. C.; Guillot, M. *J. Am. Chem. Soc.* **1991**, *113*, 5873. (b) Sessoli, R.; Tsai, H.-L.; Schake, A. R.; Wang, S.; Vincent, J. B.; Folting, K.; Gatteschi, D.; Christou, G.; Hendrickson, D. N. *J. Am. Chem. Soc.* **1993**, *115*, 1804. (c) Sessoli, R.; Gatteschi, D.; Caneschi, A.; Novak, M. A. *Nature* **1993**, *365*, 141.

(2) Villain, F.; Hartmann-Boutron, F.; Sessoli, R.; Rettori, A. *Europhys. Lett.* **1994**, *27*, 159.

(3) Much additional interest in these clusters has been generated by the observation of quantum tunneling of the magnetization: (a) Friedman, J. R.; Sarachik, M. P.; Tejada, J.; Maciejewski, J.; Ziolo, R. *J. Appl. Phys.* **1996**, *79*, 6031. (b) Friedman, J. R.; Sarachik, M. P.; Tejada, J.; Ziolo, R. *Phys Rev. Lett.* **1996**, *76*, 3830. (c) Thomas, L.; Lionti, F.; Ballou, R.; Gatteschi, D.; Sessoli, R.; Barbara, B. *Nature* **1996**, *383*, 145. (d) Hernandez, J. M.; Zhang, X. X.; Luis, F.; Tejada, J.; Friedman, J. R.; Sarachik, M. P.; Ziolo, R. *Phys Rev. B* **1997**, *55*, 5858. (e) Sangregorio, C.; Ohm, T.; Paulsen, C.; Sessoli, R.; Gatteschi, D. *Phys. Rev. Lett.* **1997**, *78*, 4645. (f) Aubin, S. M. J.; Dilley, N. R.; Pardi, L.; Krzystek, J.; Wemple, M. W.; Brunel, L.-C.; Maple, M. B.; Christou, G.; Hendrickson, D. N. *J. Am. Chem. Soc.* **1998**, *120*, 4991 and references therein.

prototype.[1,4] These species are all homometallic clusters in which the magnetic anisotropy stems from zero-field splitting associated with V^{III}, Mn^{III}, or Fe^{III} centers, and magnetic superexchange occurs through bridging oxygen atoms. In view of the difficulties in assembling predetermined structures and predicting magnetic properties, the design of metal−oxo clusters with larger barriers presents a formidable challenge. Consequently, we[5] and others[6] have begun to develop alternative cluster systems, wherein some measure of control over structures and the critical parameters S and D might be attained.

In particular, metal−cyanide cluster systems offer several advantages for achieving such control.[7] Simple ligand substitution chemistry, wherein a terminal M−CN unit reacts with an H_2O−M′ moiety to generate a linear M−CN−M′ bridge, can be employed in assembling clusters. The design of specific bimetallic constructs is then aided by the expected regularity of the cyanide bridges and metal coordination geometries. Moreover, the nature of the magnetic exchange coupling between M and M′ in the resulting cluster is readily predicted.[8] Assuming an octahedral coordination environment for both metal centers, unpaired electrons in adjacent metal orbitals of compatible symmetry ($t_{2g} + t_{2g}$ or $e_g + e_g$) will couple antiferromagnetically across the cyanide bridge, whereas those in orthogonal orbitals ($t_{2g} + e_g$) will couple ferromagnetically. The antiferromagnetic interaction is typically stronger than the ferromagnetic interaction and will dominate the superexchange in a competitive situation. Finally, when confronted with cyanide and other ligands having similar steric demands, a wide selection of transition-metal ions prefer to adopt an octahedral coordination geometry. Thus, once a new cluster geometry containing octahedral metal sites is discovered, it should generally prove possible to adjust the ground-state spin and magnetic anisotropy via substitution of appropriate metal ions.

Our approach to synthesizing high-nuclearity metal−cyanide clusters employs multidentate capping ligands to inhibit growth of an extended solid and direct the structure of the product. For example, the reaction between $[(tacn)Co(CN)_3]$ (tacn = 1,4,7-triazacyclononane) and $[(tacn)Co(H_2O)_3]^{3+}$ has been demonstrated to produce a cubic cluster, $[(tacn)_8Co_8(CN)_{12}]^{12+}$, consisting of a single cage unit excised from the Prussian blue type framework.[5a,9] Efforts to realize larger cluster geometries capable of supporting higher spin ground states have since utilized *N*,*N*′,*N*″-trimethyl-1,4,7-triazacyclononane (Me_3tacn) as a capping ligand on just one of the two reaction components.[5b−d] Accordingly, the following reaction carried out in boiling aqueous solution was found to yield a face-centered cubic cluster containing 14 metal centers.[5b]

$$8[(Me_3tacn)Cr(CN)_3] + 6[Ni(H_2O)_6]^{2+} \rightarrow [(Me_3tacn)_8Cr_8Ni_6(CN)_{24}]^{12+} \quad (1)$$

Here, the heat employed during the synthesis promotes linkage isomerization of the cyanide ligand to give a Cr^{III}−NC−Ni^{II} bridging arrangement, thereby rendering the Ni^{II} centers diamagnetic and disrupting the putative $S = 18$ ground state of the ferromagnetically coupled intermediate. Other two-component reactions have combined Me_3tacn ligated corner units with complexes of the trans-directing ligand 1,4,8,11-tetraazacyclotetradecane (cyclam), in attempts to assemble a 20-metal cluster adopting an edge-bridged cubic geometry. While formation of such a product has not yet been verified crystallographically, a cluster corresponding to a linear edge fragment with an $S = 4$ ground state was isolated from closely related reactions:[5b]

$$2[(Me_3tacn)Cr(CN)_3] + [(cyclam)Ni(H_2O)_2]^{2+} \rightarrow [(Me_3tacn)_2(cyclam)NiCr_2(CN)_6]^{2+} \quad (2)$$

Efforts to characterize additional high-nuclearity species are ongoing.

(4) (a) Barra, A.-L.; Debrunner, P.; Gatteschim, D.; Schulz, C. E.; Sessoli, R. *Europhys. Lett.* **1996**, *35*, 133. (b) Aubin, S. M. J.; Wemple, M. W.; Adams, D. M.; Tsai, H.-L.; Christou, G.; Hendrickson, D. N. *J. Am. Chem. Soc.* **1996**, *118*, 7746. (c) Castro, S. L.; Sun, Z.; Grant, C. M.; Bollinger, J. C.; Hendrickson, D. N.; Christou, G. *J. Am. Chem. Soc.* **1998**, *120*, 2365. (d) Barra, A. L.; Caneschi, A.; Cornia, A.; Fabrizi de Biani, F.; Gatteschi, D.; Sangregorio, C.; Sessoli, R.; Sorace, L. *J. Am. Chem. Soc.* **1999**, *121*, 5302. (e) Barra, A. L.; Caneschi, A.; Gatteschi, D.; Goldberg, D. P.; Sessoli, R. *J. Solid State Chem.* **1999**, *145*, 484. (f) Aubin, S. M. J.; Sun, Z.; Pardi, L.; Krzystek, J.; Folting, K.; Brunel, L.-C.; Rheingold, A. L.; Christou, G.; Hendrickson, D. N. *Inorg. Chem.* **1999**, *38*, 5329. (g) Yoo, J.; Brechin, E. K.; Yamaguchi, A.; Nakano, M.; Huffman, J. C.; Maniero, A. L.; Brunel, L.-C.; Awaga, K.; Ishimoto, H.; Christou, G.; Hendrickson, D. N. *Inorg. Chem.* **2000**, *39*, 3615. (h) Goodwin, J. C.; Sessoli, R.; Gatteschi, D.; Wernsdorfer, W.; Powell, A. K.; Heath, S. L. *J. Chem. Soc., Dalton Trans.* **2000**, 1835. (i) Benelli, C.; Cano, J.; Journaux, Y.; Sessoli, R.; Solan, G. A.; Winpenny, R. E. P. *Inorg. Chem.* **2001**, *40*, 188. (j) Boskovic, C.; Brechin, E. K.; Streib, W. E.; Folting, K.; Hendrickson, D. N.; Christou, G. *Chem. Commun.* **2001**, 467.

(5) (a) Heinrich, J. L.; Berseth, P. A.; Long, J. R. *Chem. Commun.* **1998**, 1231. (b) Berseth, P. A.; Sokol, J. J.; Shores, M. P.; Heinrich, J. L.; Long, J. R. *J. Am. Chem. Soc.* **2000**, *122*, 9655. (c) Sokol, J. J.; Shores, M. P.; Long, J. R. *Angew. Chem., Int. Ed. Engl.* **2001**, *40*, 236. (d) Heinrich, J. L.; Sokol, J. J.; Hee, A. G.; Long, J. R. *J. Solid State Chem.* **2001**, *159*, 293.

(6) (a) Mallah, T.; Auberger, C.; Verdaguer, M.; Veillet, P. *J. Chem. Soc., Chem. Commun.* **1995**, 61. (b) Scuiller, A.; Mallah, T.; Verdaguer, M.; Nivorzkhin, A.; Tholence, J.-L.; Veillet, P. *New J. Chem.* **1996**, *20*, 1. (c) Vahrenkamp, H.; Geiss, A.; Richardson, G. N. *J. Chem. Soc., Dalton Trans.* **1997**, 3643 and references therein. (d) Rajendiran, T. M.; Mathonière, C.; Golhen, S.; Ouahab, L.; Kahn, O. *Inorg. Chem.* **1998**, *37*, 2651. (e) Oshio, H.; Tamada, O.; Onodera, H.; Ito, T.; Ikoma, T.; Tero-Kubota, S. *Inorg. Chem.* **1999**, *38*, 5686. (f) Zhao, L.; Matthews, C. J.; Thompson, L. K.; Heath, S. L. *Chem. Commun.* **2000**, 265. (g) Zhong, Z. J.; Seino, H.; Mizobe, Y.; Hidai, M.; Fujishima, A.; Ohkoshi, S.; Hashimoto, K. *J. Am. Chem. Soc.* **2000**, *122*, 2952. (h) Larionova, J.; Gross, M.; Pilkington, M.; Andres, H.; Stoeckli-Evans, H.; Güdel, H. U.; Decurtins, S. *Angew. Chem., Int. Ed. Engl.* **2000**, *39*, 1605. (i) Parker, R. J.; Spiccia, L.; Berry, K. J.; Fallon, G. D.; Moubaraki, B.; Murray, K. S. *Chem. Commun.* **2001**, 333. (j) Depperman, E. C.; Bodnar, S. H.; Vostrikova, K. E.; Schultz, D. A.; Kirk, M. L. *J. Am. Chem. Soc.* **2001**, *123*, 3133. (k) Smith, J. A.; Galán-Mascarós, J.-R.; Clérac, R.; Sun, J.-S.; Ouyang, X.; Dunbar, K. R. *Polyhedron* **2001**, *20*, 1727.

(7) Many of these advantages have been exploited in manipulating the bulk magnetic properties of Prussian blue type solids: (a) Mallah, T.; Thiébaut, S.; Verdaguer, M.; Veillet, P. *Science* **1993**, *262*, 1554. (b) Entley, W. R.; Girolami, G. S. *Science* **1995**, *268*, 397. (c) Ferlay, S.; Mallah, T.; Ouahès, R.; Veillet, P.; Verdaguer, M. *Nature* **1995**, *378*, 701. (d) Sato, O.; Iyoda, T.; Fujishama, A.; Hashimoto, K. *Science* **1996**, *271*, 49. (e) Sato, O.; Iyoda, T.; Fujishama, A.; Hashimoto, K. *Science* **1996**, *272*, 704. (f) Larionova, J.; Clérac, R.; Sanchiz, J.; Kahn, O.; Golhen, S.; Ouahab, L. *J. Am. Chem. Soc.* **1998**, *120*, 13088. (g) Holmes, S. M.; Girolami, G. S. *J. Am. Chem. Soc.* **1999**, *121*, 5593. (h) Hatlevik, Ø.; Buschmann, W. E.; Zhang, J.; Manson, J. L.; Miller, J. S. *Adv. Mater.* **1999**, *11*, 914.

(8) (a) Entley, W. R.; Treadway, C. R.; Girolami, G. S. *Mol. Cryst. Liq. Cryst.* **1995**, *273*, 153. (b) Weihe, H.; Güdel, H. U. *Comments Inorg. Chem.* **2000**, *22*, 75.

(9) Analogous cubic clusters featuring cyclopentadienyl and carbonyl ligands have also been prepared: (a) Klausmeyer, K. K.; Rauchfuss, T. B.; Wilson, S. R. *Angew. Chem., Int. Ed. Engl.* **1998**, *37*, 1694. (b) Klausmeyer, K. K.; Wilson, S. R.; Rauchfuss, T. B. *J. Am. Chem. Soc.* **1999**, *121*, 2705.

(10) (a) Singer, L. S. *J. Chem. Phys.* **1955**, *23*, 379. (b) Elbers, G.; Remme, S.; Lehmann, G. *Inorg. Chem.* **1986**, *25*, 896.

(11) (a) Gregson, A. K.; Anker, M. *Aust. J. Chem.* **1979**, *32*, 503. (b) Averill, B. A.; Orme-Johnson, W. H. *Inorg. Chem.* **1980**, *19*, 1702.

(12) Backes-Dahman, G.; Herrman, W.; Wieghardt, K.; Weiss, J. *Inorg. Chem.* **1985**, *24*, 485.

(13) Markley, T. J.; Toby, B. H.; Pearlstein, R. M.; Ramprasad, D. *Inorg. Chem.* **1997**, *36*, 3376.

(14) (a) Bosnich, B.; Tobe, M. L.; Webb, G. A. *Inorg. Chem.* **1965**, *4*, 1109. (b) Iwamoto, E.; Imai, K.; Yamamoto, K. *Inorg. Chem.* **1984**, *23*, 986.

(15) As discussed below, the results of elemental analysis, X-ray crystallography, and mass spectrometry in combination suggest that this product is contaminated with a slight amount of $[(Me_3tacn)_2Mo_2(CN)_4Cl](BPh_4)$. Presumably, an impurity in the LiCN·DMF serves as a source of chloride ions.

Although the metal complexes used in these exploratory assembly reactions represent stable species that are easily prepared and manipulated, they are not necessarily expected to impart significant magnetic anisotropy to the resulting clusters. To achieve the desired anisotropy, one viable strategy is to incorporate analogous complexes of metal ions known to exhibit a large single-ion anisotropy, such as those inherent to proven single-molecule magnets: V^{III}, high-spin Mn^{III}, and high-spin Fe^{III}. Another idea, however, is to move down the periodic table and utilize complexes of second- and third-row transition-metal ions, for which the greater spin−orbit coupling increases the magnitude of the zero-field splitting. Thus, for example, whereas $[Cr(acac)_3]$ has an axial zero-field splitting of magnitude $|D| = 0.59$ cm^{-1},[10] $[Mo(acac)_3]$ exhibits a large negative D value of -6.3 cm^{-1}.[11] Indeed, replacing Cr^{III} centers with Mo^{III} centers would provide a means of increasing the magnetic anisotropy of a cluster without altering its ground state spin. Furthermore, the radially extended valence *d* orbitals of Mo^{III} would be expected to have greater overlap with the cyanide-based orbitals, leading to stronger magnetic exchange coupling and a spin ground state that is more isolated in energy. Herein we establish the validity of this approach with the synthesis of $[(Me_3tacn)Mo(CN)_3]$ and demonstration of its ability to replace $[(Me_3tacn)Cr(CN)_3]$ in eqs 1 and 2 above.

Experimental Section

Preparation of Compounds. Preparations of compounds **1**−**3** were carried out under a pure dinitrogen atmosphere; all other preparations were conducted in air. Crude Me_3tacn obtained from Unilever was purified by vacuum distillation (36 °C, ca. 80 mTorr) prior to use. The compounds $[(Me_3tacn)MoBr_3]$,[12] LiCN·DMF,[13] and $[Ni(cyclam)X_2]$ ($X = Br^-$, I^-, ClO_4^-)[14] were synthesized as described previously. Water was distilled and deionized with a Milli-Q filtering system. Diethyl ether and tetrahydrofuran were passed through alumina and degassed prior to use. Acetonitrile was distilled over CaH_2 and degassed prior to use. All other reagents were obtained from commercial vendors and used without further purification.

$[(Me_3tacn)Mo(CF_3SO_3)_3]$ (1). A 150-mL Schlenck flask was fitted with an oil bubbler and charged with a magnetic stir bar and solid $[(Me_3tacn)MoBr_3]$ (5.5 g, 11 mmol). Under a flow of dinitrogen, trifluoromethanesulfonic acid (16 mL, 0.18 mol) was added to form a deep red-purple solution. The solution was stirred and heated at 140 °C for 4 days, producing a dark brown solution. The solution was then allowed to cool to room temperature, and 200 mL of Et_2O was added to precipitate a brown solid. The solid was filtered, washed with 50 mL of Et_2O, and dried under dinitrogen to yield 7.7 g (99%) of light tan product. IR: ν_{SO} 1189 cm^{-1}. Anal. Calcd. for $C_{12}H_{21}F_9MoN_3O_9S_3$: C, 20.17; H, 2.96; N, 5.88; S, 13.46. Found: C, 20.05; H, 2.91; N, 5.78; S, 13.26.

$[(Me_3tacn)Mo(CN)_3]$ (2). Solid LiCN·DMF (0.910 g, 8.43 mmol) was added to a solution of **1** (2.00 g, 2.80 mmol) in 3.5 mL of DMF. The resulting dark brown solution was stirred at room temperature for 2 days, whereupon a light tan precipitate formed. The solid was collected by filtration, washed with THF (2 × 10 mL) and Et_2O (2 × 10 mL), and dried under dinitrogen to afford 0.388 g (40%) of product. Absorption spectrum (H_2O): λ_{max} (ϵ_M) 410 (48, sh), 490 (28, sh), 631 (18) nm. IR: ν_{CN} 2098, 2090 cm^{-1}. μ_{eff} (295 K) 3.59 μ_B. Anal. Calcd. for $C_{12}H_{21}MoN_6$: C, 41.74; H, 6.13; N, 24.34. Found: C, 41.67; H, 6.30; N, 24.21. Brown block-shaped crystals of **2**·H_2O suitable for X-ray analysis were grown by slow evaporation of a concentrated aqueous solution of the product.

$Li[(Me_3tacn)Mo(CN)_4]$ (3). Solid LiCN·DMF (3.0 g, 28 mmol) was added to a stirring solution of **1** (2.2 g, 3.1 mmol) in 6 mL of DMF. The resulting brown solution was stirred for 3 days to afford a tan solid under a brown supernatant solution. The solid was collected by filtration, washed with successive aliquots of DMF (5 mL), THF (3 × 10 mL), and Et_2O (15 mL), and dried in a dinitrogen atmosphere to give 0.97 g (83%) of product. Absorption spectrum (H_2O): λ_{max} (ϵ_M) 359 (93, sh), 392 (71, sh) nm. IR: ν_{CN} 2116, 2104, 2080, 2061 cm^{-1}. μ_{eff} (295 K) 2.47 μ_B. Anal. Calcd. for $C_{13}H_{21}MoLiN_7$: C, 41.28; H, 5.60; N, 25.92. Found: C, 40.97; H, 5.61; N, 25.53. Orange rod-shaped crystals of **3**·2MeOH suitable for X-ray analysis were obtained by diffusion of Et_2O into a concentrated solution of the product in methanol.

$[(Me_3tacn)Mo(O)(CN)_2]$ (4). Compound **3** (0.20 g, 0.52 mmol) was dissolved in 10 mL of water to form a brown solution. In the course of heating at reflux for 1 day in air, the solution gradually changed color from brown to green and, finally, to pale blue. After reducing the volume of the solution to 1 mL, 5 mL of THF was added to precipitate a white solid. The solution was collected by filtration and reduced to dryness in vacuo. Addition of 5 mL of 95% EtOH gave a pale blue solution over a white solid. Upon centrifugation, the solution was decanted and then evaporated to dryness to afford a pale blue solid (80 mg) containing the product. IR: ν_{CN} 2106, 2091, 2083 cm^{-1}; ν_{MoO} 952 cm^{-1}. Elemental analysis indicated this compound to be slightly impure; however, further purification was not attempted. Pale blue platelike crystals of **4**·H_2O suitable for X-ray analysis were obtained by allowing a concentrated aqueous solution of the solid to evaporate slowly.

$[(Me_3tacn)_2Mo_2(CN)_5](BPh_4)$ (5). A reaction between LiCN·DMF (0.23 g, 2.1 mmol) and **1** (0.60 g, 0.84 mmol) was carried out using a procedure analogous to that described in the preparation of **2** above. The ensuing gray-tan solid was dissolved in water, and a solution of $NaBPh_4$ (0.13 g, 0.38 mmol) in 1 mL of H_2O was added to afford a brown precipitate. The solid was collected by filtration, washed with successive aliquots of water (3 × 10 mL), and dried in air to give 0.040 g (10%) of product.[15] IR: ν_{CN} 2100, 2060 cm^{-1}. Anal. Calcd. for $C_{47}H_{62}BMo_2N_{11}$: C, 57.38; H, 6.35; N, 15.66. Found: C, 56.52; H, 6.59; N, 14.54. Brown rod-shaped crystals suitable for X-ray analysis were grown by diffusion of Et_2O into a concentrated solution of the product in acetonitrile.

$[(Me_3tacn)_8Mo_8Ni_6(CN)_{24}]Br_{12}\cdot 27H_2O$ (6). A solution of $NiBr_2\cdot 6H_2O$ (59 mg, 0.18 mmol) in 2 mL of water was added to a saturated solution of **2** (75 mg, 0.22 mmol) in 3 mL of water. The resulting yellow solution was stirred and heated until its volume was reduced to 2 mL. Upon cooling to room temperature, a yellow solid precipitated. The solid was collected by filtration, washed with 10 mL of acetone and 5 mL of Et_2O, and dried in air to give 96 mg of product. Further concentration of the mother liquor to ca. 0.5 mL produced a second crop of product, for a total yield of 100 mg (80%). Absorption spectrum (H_2O): λ_{max} (ϵ_M) 254 (65200), 305 (27900, sh), 335 (16500, sh), 380 (7560, sh) nm. IR: ν_{CN} 2152 (sh), 2127, 2090 (sh) cm^{-1}. ES^+-MS: *m*/*z* 1278 ([**6** − 3Br − 27H_2O]$^{3+}$). Anal. Calcd. for $C_{96}H_{222}Br_{12}Mo_8N_{48}Ni_6O_{27}$: C, 25.29; H, 4.91; N, 14.74. Found: C, 25.53; H, 4.78; N, 14.46. The water content of this compound was confirmed by thermogravimetric analysis. Orange block-shaped crystals of **6**·3H_2O suitable for X-ray analysis were grown by slow evaporation of an aqueous solution of the product.

$[(Me_3tacn)_8Mo_8Ni_6(CN)_{24}]I_{12}\cdot 18H_2O$ (7). Solid NiI_2 (0.23 g, 0.74 mmol) was added to a solution of **2** (0.33 g, 0.96 mmol) in 50 mL of water. The mixture was stirred and heated at reflux for 1 h to obtain a deep orange-red solution. A small amount of solid was separated from the solution by filtration. The filtrate was concentrated to a volume of 25 mL by heating and then cooled to room temperature to precipitate an orange microcrystalline powder. The solid was collected by filtration, washed with acetone (2 mL) and Et_2O (2 mL), and dried in air to afford 0.31 g of product. Further concentration of the mother liquor to a volume of 5 mL produced a second crop of product, for a total yield of 0.35 g (59%). ES^+-MS: *m*/*z* 646 ([**7**−6I−18H_2O]$^{6+}$), 800 ([**7**−5I−18H_2O]$^{5+}$), 1032 ([**7**−4I−18H_2O]$^{4+}$). IR: ν_{CN} 2147 (sh), 2123, 2085

(sh) cm^{-1}. Anal. Calcd. for $C_{96}H_{204}I_{12}Mo_8N_{48}Ni_6O_{18}$: C, 23.24; H, 4.14; N, 13.55. Found: C, 23.34; H, 4.17; N, 13.32. The water content of this compound was confirmed by thermogravimetric analysis. Crystals of **7**·9H_2O suitable for X-ray analysis were grown by slow evaporation of an aqueous solution of the product.

[α-(Me_3tacn)$_2$(cyclam)$NiMo_2(CN)_6$]I_2 (8). Solid [Ni(cyclam)I_2] (82 mg, 0.16 mmol) was added to a saturated solution of **2** (100 mg, 0.30 mmol) in 5 mL of MeCN, whereupon the mixture darkened in color. The mixture was stirred for 33 h and then filtered to give a light tan powder and a brown filtrate. The solid was washed with successive aliquots of MeCN (1 mL), Et_2O (2 × 10 mL), THF (5 mL), and Et_2O (2 × 10 mL) and dried in air to afford 0.17 g (95%) of product. IR: ν_{CN} 2245, 2220, 2118, 2091 cm^{-1}. Anal. Calcd. for $C_{34}H_{66}I_2Mo_2N_{16}$-Ni: C, 33.94; H, 5.53; N, 18.62. Found: C, 34.05; H, 5.67; N, 18.26. Crystals of **8**·2DMF suitable for X-ray analysis were grown by diffusion of Et_2O into a concentrated solution of the product in DMF.

[β-(Me_3tacn)$_2$(cyclam)$NiMo_2(CN)_6$]I_2·6H_2O (9). Solid [Ni(cyclam)-I_2] (82 mg, 0.16 mmol) was added to a solution of **2** (110 mg, 0.32 mmol) in 25 mL of water. The brown solution was stirred and heated at reflux until its volume was reduced to 2 mL. It was then cooled to room temperature and further concentrated to a volume of 1 mL by evaporation upon standing in air. After standing overnight at 5 °C, large brown crystals had formed. These were collected by filtration, washed with Et_2O (10 mL), and dried in air to afford 0.14 g (69%) of brown microcrystalline product. IR: ν_{CN} 2127, 2110, 2098 cm^{-1}. Anal. Calcd. for $C_{34}H_{78}I_2Mo_2N_{16}NiO_6$: C, 31.14; H, 5.99; N, 17.09. Found: C, 31.04; H, 5.98; N, 16.83. The water content of this compound was confirmed by thermogravimetric analysis. Crystals of **9**·H_2O suitable for X-ray analysis were grown by slow evaporation of an aqueous solution of the product.

[α-(Me_3tacn)$_2$(cyclam)$NiMo_2(CN)_6$]Br_2·6H_2O (10). This compound was prepared from [Ni(cyclam)Br_2] (0.15 g, 0.36 mmol) and **2** (0.24 g, 0.69 mmol) by a procedure analogous to that described for the preparation of **9**. The product was obtained as 0.24 g (57%) of brown, X-ray-quality crystals and microcrystalline solid. IR: ν_{CN} 2127, 2114, 2096, 2089 cm^{-1}. Anal. Calcd. for $C_{34}H_{78}Br_2Mo_2N_{16}NiO_6$: C, 33.54; H, 6.46; N, 18.41. Found: C, 33.21; H, 6.39; N, 18.05. The water content of this compound was confirmed by thermogravimetric analysis.

[β-(Me_3tacn)$_2$(cyclam)$NiMo_2(CN)_6$]$(ClO_4)_2$·2H_2O (11). A 5 mL aqueous solution of [Ni(cyclam)]$(ClO_4)_2$ (83 mg, 0.18 mmol) was added to a stirring solution of **2** (0.12 g, 0.36 mmol) in 5 mL of water. The resulting golden brown solution was stirred and heated in air until its volume was reduced to 4 mL. Upon cooling to room temperature, orange-brown crystals formed. These were collected by filtration, washed with 5 mL of Et_2O, and dried in air to afford 0.15 g (71%) of brown microcrystalline product. IR: ν_{CN} 2112, 2089 cm^{-1}. ES^+-MS: *m*/*z* 1049 ([**11**−ClO_4]$^{1+}$). Anal. Calcd. for $C_{34}H_{70}Cl_2Mo_2N_{16}NiO_{10}$: C, 34.48; H, 5.96; N, 18.92. Found: C, 34.33; H, 5.88; N, 18.54. The water content of this compound was confirmed by thermogravimetric analysis. *Caution!* When fully dehydrated by heating to temperatures above 210 °C, this compound can decompose explosively. Crystals suitable for X-ray analysis were obtained by slow evaporation of an aqueous solution of the product.

[(Me_3tacn)$_2$(cyclam)$NiMo_2(O)_2(CN)_4$]I_2·6H_2O (12). Solid [Ni-(cyclam)I_2] (45 mg, 0.088 mmol) was added to a solution of **2** (45 mg, 0.13 mmol) in 15 mL of water. The resulting brown solution was stirred and heated at reflux until its volume was reduced to 5 mL. It was then cooled to room temperature and further concentrated to 1 mL by evaporation upon standing in air. After standing overnight at room temperature, blue-green crystals suitable for X-ray analysis had formed. The solid was collected by filtration, washed with successive aliquots of cold water (1 mL) and Et_2O (5 mL), and dried in air to afford 41 mg (49%) of product. IR: ν_{CN} 2109, 2098 cm^{-1}. Anal. Calcd. for $C_{32}H_{78}I_2Mo_2N_{14}NiO_8$: C, 29.76; H, 6.09; N, 15.18. Found: C, 30.02; H, 6.12; N, 15.18.

[(Me_3tacn)$_2$(cyclam)$_3$(H_2O)$_2$$Ni_3Mo_2(CN)_6$]$Br_6$·9$H_2O$ (13). Compound **2** (26.0 mg, 0.0753 mmol) and [Ni(cyclam)Br_2] (0.160 g, 0.382 mmol) were dissolved in 10 mL of water and heated to reflux to produce a brown solution. The solution was concentrated to a volume of 1 mL and then allowed to evaporate to dryness by standing overnight at room temperature. Brown crystals of **13**·5H_2O suitable for X-ray analysis were obtained, along with violet crystals of [Ni(cyclam)Br_2]. This compound only formed quantitatively from solutions containing a large excess of [Ni(cyclam)Br_2], and all attempts at cleanly separating the product were unsuccessful. Consequently, all measurements were performed on a finely ground mixture containing **13** and [Ni(cyclam)-Br_2] in a 1.00:7.13 molar ratio. IR: ν_{CN} 2121, 2107 cm^{-1}. Anal. Calcd. for $C_{125.30}H_{307.12}Br_{20.26}Mo_2N_{52.52}Ni_{10.13}O_{11}$: C, 29.33; H, 6.03; N, 14.34. Found: C, 29.45; H, 6.32; N, 13.95. The water content of this compound was confirmed by thermogravimetric analysis.

[(Me_3tacn)(cyclam)$NiMo(CN)_3$]I_2·4H_2O (14). Solid [Ni(cyclam)-I_2] (90 mg, 0.18 mmol) was added to a solution of **2** (60 mg, 0.17 mmol) in 5 mL of water. The brown solution was stirred and heated at reflux until its volume was reduced to 2 mL. The solution was allowed to stand at room-temperature overnight, whereupon yellow-brown rod-shaped crystals suitable for X-ray analysis formed. The crystals were collected by filtration, washed with 5 mL of Et_2O, and dried in air to afford 64 mg (40%) of product. IR: ν_{CN} 2121, 2117, 2102 cm^{-1}. Anal. Calcd. for $C_{22}H_{53}I_2MoN_{10}NiO_4$: C, 28,41; H, 5.74; N, 15.06. Found: C, 28.41; H, 5.81; N, 14.73.

[(Me_3tacn)(cyclam)$NiMo(CN)_3$]$(ClO_4)_2$·1.5H_2O (15). Solid [Ni-(cyclam)]$(ClO_4)_2$ (70 mg, 0.15 mmol) was added to a solution of **2** (52 mg, 0.15 mmol) in 5 mL of water. The resulting yellow solution was concentrated to a volume of 3 mL by heating and was then allowed to cool to room temperature. Upon standing overnight, brown rod-shaped crystals suitable for X-ray analysis formed. The crystals were collected by filtration, washed with 2 mL of Et_2O, and dried in air to afford 71 mg (56%) of product. IR: ν_{CN} 2116, 2102 cm^{-1}. Anal. Calcd. for $C_{22}H_{48}Cl_2MoN_{10}NiO_{9.5}$: C, 31.49; H, 5.89; N, 16.87. Found: C, 31.63; H, 5.83; N, 16.48. *Caution!* This perchlorate-containing compound poses an explosion hazard, and should only be handled with care and in small quantities.

X-ray Structure Determinations. Structures were determined for compounds **2**−**15** (see the Supporting Information). Single crystals were coated with Paratone-N oil, attached to glass fibers, transferred to a Siemens SMART diffractometer, and cooled in a dinitrogen stream. Initial lattice parameters were obtained from a least-squares analysis of more than 30 carefully centered reflections; these parameters were later refined against all data. None of the crystals showed significant decay during data collection. Data were integrated and corrected for Lorentz and polarization effects using SAINT and were corrected for absorption effects using SADABS.

Space group assignments were based on systematic absences, *E* statistics, and successful refinement of the structures. Structures were solved by direct methods with the aid of successive difference Fourier maps and were refined against all data using the SHELXTL 5.0 software package. Thermal parameters for all atoms with $Z > 3$ were refined anisotropically, except for those disordered over multiple partially occupied sites in the structures of **6**·3H_2O, **7**·9H_2O, **9**·H_2O, **11**, **13**, and **15**. In the structure of compound **8**·2DMF, the positions of the hydrogen atoms bound to the methyl carbons in the Me_3tacn ligand and DMF solvate molecule as well as the nitrogen atoms of the cyclam ligand were located in the difference Fourier map and were refined using isotropic thermal parameters. Hydrogen atoms associated with solvate water molecules and disordered methylene carbon atoms (with the exception of those in **15**) were not included in the structural refinements. All other hydrogen atoms were assigned to ideal positions and refined using a riding model with an isotropic thermal parameter 1.2 times that of the attached carbon or nitrogen atom (1.5 times for methyl hydrogens). In the structure of **3**·2MeOH, all carbon and nitrogen atoms located within 1.7 Å of each other were restrained to

have the same U_{ij} parameters. In the structure of **5**, the positions of the C and N atoms in the bridging cyanide ligand are disordered. An occupancy factor of 0.5C + 0.5N was assigned to each of the two cyanide atom sites, and their thermal parameters were refined anisotropically. Methylene carbon atoms in the structures of **6**·3H_2O, **7**·9H_2O, and **15** were modeled as being disordered over two equally occupied positions, corresponding to two distinct Me_3tacn ligand conformations. One methyl carbon atom and one nitrogen atom in the structure of **15** were modeled similarly. Three of the bromide anions and all of the solvate water molecules in the structure of **6**·3H_2O were modeled as being disordered over multiple positions. Two of the iodide anions and all of the solvate water molecules in **7**·9H_2O were treated similarly, as were all of the solvate water molecules in **9**·H_2O, three oxygen atoms of the perchlorate anion and one solvate water molecule in **11**, three solvate water molecules in **13**, and one chlorine and seven oxygen atoms of perchlorate anions and all of the solvate water molecules in **15**. The final agreement factors for the structures of **6**·3H_2O, **7**·9H_2O, and **15** are high owing to the extensive disorder present in the crystals and the accompanying poor quality of the data. The program CHECKCIF revealed no crystallographic errors for these structures.

Magnetic Susceptibility Measurements. DC magnetic susceptibility data were collected using a Quantum Design MPMS2 SQUID magnetometer at temperatures ranging from 5 to 295 K. Data were corrected for diamagnetic contributions using Pascal's constants. A temperature-independent paramagnetism of $100 \cdot 10^{-6}$ cgsu per Mo center and $200 \cdot 10^{-6}$ cgsu per Ni center was assumed for each compound. Samples for magnetization measurements were suspended in a petroleum jelly mull to prevent torquing of the crystallites at high magnetic fields. Susceptibility data were fit with theoretical models using a relative error minimization routine (MAGFIT 3.1),[16] except in the cases of **11** and **13**−**15**, where data were simulated using MAGPACK.[17] Reported coupling constants are based on exchange Hamiltonians of the form $\hat{H} = -2J\hat{S}_i \cdot \hat{S}_j$.

A computer program (ANISOFIT) for fitting magnetization data was developed for use in estimating the zero-field splitting parameters of high-spin clusters. The program is implemented on the MATLAB platform and assumes that only the spin ground state of the molecule is populated, that **g** is isotropic, and that the principal axes of **D** and **g** coincide. Accordingly, it utilizes a spin Hamiltonian with the following form.

$$\hat{H} = D\hat{S}_z^2 + E(\hat{S}_x^2 + \hat{S}_y^2) + g\mu_B \mathbf{S}\cdot\mathbf{B} \qquad (3)$$

The program REPULSION[18] is employed in generating a set of points, $\{\theta, \phi\}$, evenly distributed over the surface of a sphere, which is then used to perform numerical integration over the Boltzmann distribution.[19] The calculated values of *D*, *E*, and *g* are optimized relative to the data through a least-squares minimization routine based on the Nelder−Mead method. Data at all applied magnetic fields were utilized simultaneously. The ideas presented by Day were closely followed throughout the course of its development.[20] This program will be made available over the Internet at http://alchemy.cchem.berkeley.edu.

Other Physical Measurements. Absorption spectra were measured with a Hewlett-Packard 8453 spectrophotometer. Infrared spectra were recorded on a Nicolet Avatar 360 FTIR spectrometer equipped with an attenuated total reflectance accessory. Mass spectrometric measurements were performed in the positive ion mode on a VG Quattro (Micromass) spectrometer or on a Bruker Apex II 7 T actively shielded FTICR mass spectrometer, both of which were equipped with an analytical electrospray ion source instrument. Thermogravimetric analyses were carried out in a dinitrogen atmosphere using a TA Instruments TGA 2950. Electrochemical measurements were conducted with a Bioanalytical Systems CV-50 potentiostat with platinum disk working, platinum wire auxiliary, and silver wire reference electrodes. Samples were measured with 0.1 M Bu_4NBF_4 as the supporting electrolyte, and ferrocene was added as an internal reference after each measurement.

Results and Discussion

Synthesis of [(Me_3tacn)Mo(CN)$_3$]. Overall, the route utilized in the preparation of [(Me_3tacn)Mo(CN)$_3$] is similar to that employed previously for the synthesis of [(Me_3tacn)Cr(CN)$_3$].[5b,21] The complex [(Me_3tacn)$MoBr_3$][12] reacts with neat triflic acid to give [(Me_3tacn)Mo(CF_3SO_3)$_3$] (**1**) in excellent yield, although significantly more forcing conditions are required to complete the substitution than those implemented in the analogous preparation of [(Me_3tacn)Cr(CF_3SO_3)$_3$].[5b,21,22] Compound **1** then serves as a useful precursor for introducing cyanide as a ligand. This process is complicated, however, by the larger radius of Mo^{III} and its propensity for adopting coordination numbers greater than six. Indeed, the only homoleptic cyanide complex of Mo^{III} that has been structurally characterized to date is the pentagonal bipyramidal species $[Mo(CN)_7]^{4-}$.[23] Consequently, the preparation of [(Me_3tacn)Mo(CN)$_3$] from the triflate complex depends critically on the number of equivalents of cyanide added in the reaction.

Use of an excess of LiCN leads to formation of Li[(Me_3tacn)Mo(CN)$_4$] (**3**). This compound contains the seven-coordinate complex $[(Me_3tacn)Mo(CN)_4]^{1-}$, as revealed in the crystal structure of **3**·2MeOH (Figure 1b). The complex adopts a monocapped octahedral geometry, in which a cyanide ligand caps and distends the triangular face opposite to the Me_3tacn ligand in the molybdenum coordination sphere. A slight distortion of the molecule away from its maximal point group symmetry of C_{3v} (ignoring tacn ring conformations) appears to originate from interactions between two of the cyanide ligands and Li^+ ions, which link the complexes into one-dimensional chains. Selected mean interatomic distances and angles from the crystal structure are listed in Table 1. Notably, there is some variation in the Mo−C distances, which fall within the range 2.075(12)−2.129(11) Å and are slightly shorter than those observed for $[Mo(CN)_7]^{4-}$ (2.157−2.164 Å).[23] At room temperature, **3** exhibits an effective magnetic moment of 2.47 μ_B. Surprisingly, this is higher than the moment of 1.80 μ_B measured for anhydrous $K_4[Mo(CN)_7]$, which clearly indicates a low-spin $S = 1/2$ electron configuration.[24] The effective moment of **3** is too low to be consistent with a high-spin $S = 3/2$ electron configuration, and yet a variable temperature measurement yielded no evidence for spin-equilibrium behavior. Thus, the moment may indicate the presence of some unidentified paramagnetic impurity in samples of **3**.

Related reactions employing fewer than 3 equiv of LiCN result in products contaminated by higher-nuclearity molybdenum−cyanide species. With the use of just 2.5 equiv, a dinuclear complex precipitates from the reaction mixture and can then be crystallized as [(Me_3tacn)$_2Mo_2$(CN)$_5$](BPh_4) (**5**). As depicted

(16) Schmitt, E. A., Ph.D. Thesis, University of Illinois at Urbana-Champaign, 1995.
(17) Borrás-Almenar, J. J.; Clemente-Juan, J. M.; Coronado, E.; Tsukerblat, B. S. *J. Comput. Chem.* **2001**, *22*, 985.
(18) Bak, M.; Nielsen, N. C. *J. Magn. Reson.* **1997**, *125*, 132.
(19) (a) Vermaas, A.; Groeneveld, W. L. *Chem. Phys. Lett.* **1974**, *27*, 583. (b) Marathe, V. R.; Mitra, S. *Chem. Phys. Lett.* **1974**, *27*, 103.
(20) Day, E. P. *Methods Enzymol.* **1993**, *227*, 437.
(21) Shores, M. P.; Berseth, P. A.; Long, J. R. *Inorg. Synth.*, submitted for publication.
(22) Ryu, C. K.; Lessard, R. B.; Lynch, D.; Endicott, J. F. *J. Phys. Chem.* **1989**, *93*, 1752.
(23) Hursthouse, M. B.; Malik, K. M. A.; Soares, A. M.; Gibson, J. F.; Griffith, W. P. *Inorg. Chim. Acta* **1980**, *45*, 81.
(24) Rossman, G. R.; Tsay, F.-D.; Gray, H. B. *Inorg. Chem.* **1973**, *12*, 824.

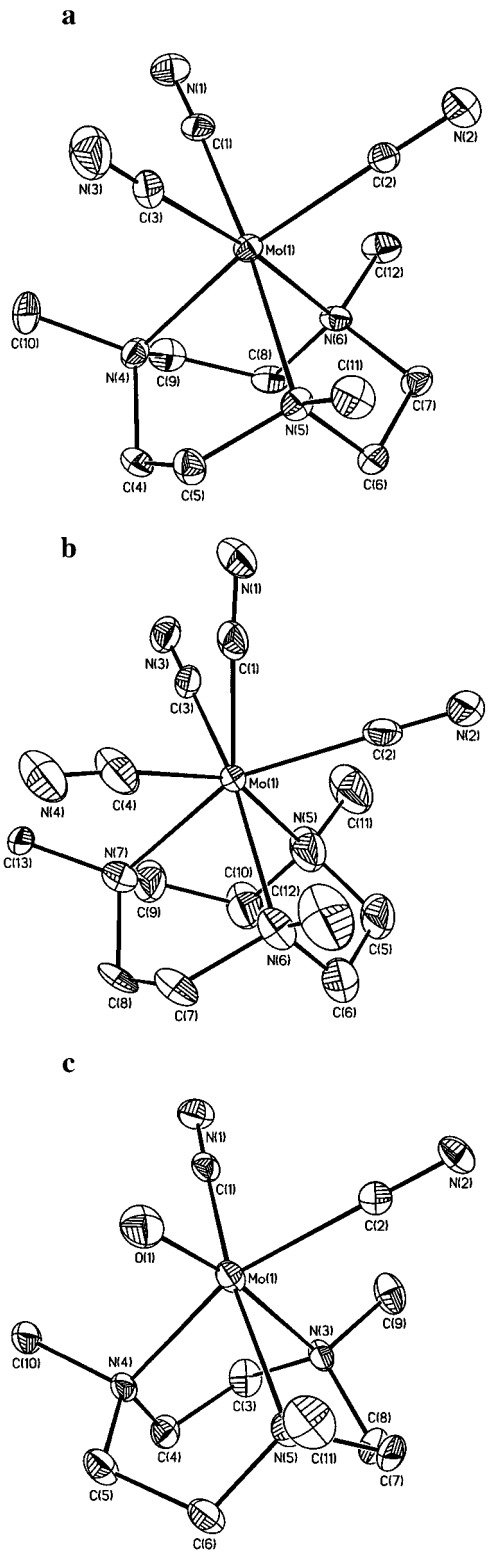

Figure 1. Structures of the mononuclear complexes $[(Me_3tacn)Mo(CN)_3]$ (a), $[(Me_3tacn)Mo(CN)_4]^{1-}$ (b), and $[(Me_3tacn)Mo(O)(CN)_2]$ (c) in $\mathbf{2}\cdot H_2O$, $\mathbf{3}\cdot 2MeOH$, and $\mathbf{4}\cdot H_2O$, respectively, showing 40% probability ellipsoids. H atoms are omitted for clarity.

in Figure 2, its structure features two octahedral Mo^{III} centers, each coordinated by a Me_3tacn group, two terminal cyanide ligands, and either the carbon or nitrogen end of a bridging cyanide ligand. The central cyanide bridge is almost perfectly linear, and the two Me_3tacn ligands are disposed in an anti conformation. Selected interatomic distances and angles are

Table 1. Selected Mean Interatomic Distances (Å) and Angles (deg) for the Mo Complexes in the Structures of $[(Me_3tacn)Mo(CN)_3]\cdot H_2O$ ($\mathbf{2}\cdot H_2O$), $Li[(Me_3tacn)Mo(CN)_4]\cdot 2MeOH$ ($\mathbf{3}\cdot 2MeOH$), and $[(Me_3tacn)Mo(O)(CN)_2]\cdot H_2O$ ($\mathbf{4}\cdot H_2O$)[a]

	$[(Me_3tacn)Mo(CN)_3]$	$[(Me_3tacn)Mo(CN)_4]^{1-}$	$[(Me_3tacn)Mo(O)(CN)_2]$
Mo−C	2.15(1)	2.11(1)	2.14(2)
Mo−N	2.227(6)	2.229(3)	2.23(2)[b]
			2.403(9)[c]
Mo−O			1.71(4)
$C-N_{CN}$	1.16(1)	1.16(1)	1.14(2)
Mo−C−N	176.8(5)	177(2)	176(1)
C−Mo−C	91(2)	71(5)[d]	91(2)
		109(12)[e]	
C−Mo−N	94(2)	84(5)[e]	89(4)
	172(1)	134(10)[d]	160.4(7)
C−Mo−O			99.3(9)
N−Mo−N	79.3(1)	76.9(7)	76(2)
N−Mo−O			99(2)
			172(1)

[a] N_{CN} indicates a N atom in a cyanide ligand. [b] N atoms located cis to the O atom. [c] N atom located trans to the O atom. [d] Angles involving atom C(1). [e] Angles not involving atom C(1).

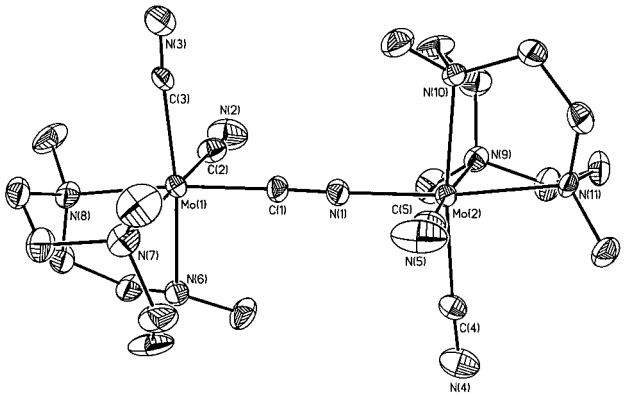

Figure 2. Structure of the $[(Me_3tacn)_2Mo_2(CN)_5]^{1+}$ cluster in **5**, showing 40% probability ellipsoids. H atoms are omitted for clarity. The bridging cyanide ligand is disordered between two orientations: the one depicted and one in which the positions of atoms C(1) and N(1) are interchanged. Selected interatomic distances (Å) and angles (°): Mo(1)−C(1) 2.020(5), mean of other Mo−C 2.15(1), Mo(2)−N(1) 2.029(6), mean $Mo-N_{tacn}$ 2.220(10), C(1)−N(1) 1.181(7), mean of other $C-N_{CN}$ 1.11(2), mean Mo−C−N 177(1), mean C−Mo−C 91.3(9), C(4)−Mo(2)−N(1) 92.2(2), C(5)−Mo(2)−N(1) 92.1(2), mean $C-Mo-N_{tacn}$ 94(1), 172(1), N(1)−Mo(2)−N(9) 95.8(2), N(1)−Mo(2)−N(10) 94.1(2), mean $N_{tacn}-Mo-N_{tacn}$ 79.6(3).

listed in the figure legend. Significantly, the C−N distances within the terminal cyanide ligands are anomalously short. We attribute this phenomenon to the presence of a small amount of compositional disorder in the crystal, in which a chloride ligand—presumably originating from the LiCl used to prepare LiCN·DMF—is occasionally present in place of a cyanide ligand. The effects of such disorder have been studied systematically for a series of crystals of composition $[HB(3\text{-}Bu^tpz)_3]Zn(CN)_{1-x}Cl_x$,[25] and are in good agreement with our own results. Furthermore, such a conclusion is supported by the slight discrepancies in the elemental analysis of **5**, as well as by the observation of a minor peak corresponding to $[(Me_3tacn)_2Mo_2(CN)_4Cl]^{1+}$ in the electrospray mass spectrum of the compound. Irrespective of the disorder, certain aspects of the crystal structure suggest the presence of strong π interactions between the molybdenum centers and the bridging cyanide ligand. The slightly elongated C−N and short Mo−C/N distances associated with the cyanide bridge are consistent with

(25) Yoon, Y.; Parkin, G. *Inorg. Chem.* **1992**, *31*, 1656.

π-back-bonding. In addition, the perpendicular metal−ligand axes are essentially coparallel for the two molybdenum centers, as reflected in the C(2)−Mo(1)−Mo(2)−C(5) and C(3)−Mo(1)−Mo(2)−C(4) torsion angles of 172.8° and 174.6°, respectively. A very strong antiferromagnetic exchange interaction between the Mo^{III} centers can therefore be expected; however, characterization of the magnetic properties of the complex awaits its further purification.

Addition of precisely 3 equiv of LiCN to a DMF solution of $[(Me_3tacn)Mo(CF_3SO_3)_3]$ yields the desired product $[(Me_3tacn)Mo(CN)_3]$ (**2**). The crystal structure of **2**·H_2O shows the octahedral complex (Figure 1a) to be isostructural with $[(Me_3tacn)Cr(CN)_3]$;[5b] selected mean interatomic distances and angles are listed in Table 1. As expected, the larger radius of molybdenum leads to longer M−C and M−N bonds and smaller N−M−N angles. Surprisingly, the Mo−C distances, which range between 2.138(5) Å and 2.159(4) Å, are actually longer than those observed in the seven-coordinate complex $[(Me_3tacn)Mo(CN)_4]^{1-}$. Compound **2** is soluble in highly polar solvents such as methanol, acetonitrile, water, DMF, and DMSO. Its cyclic voltammogram in DMF shows a reversible reduction wave corresponding to the $[(Me_3tacn)Mo(CN)_3]^{0/1-}$ couple at $E_{1/2} = -1.895$ V ($\Delta E_p = 128$ mV) versus Cp_2Fe/Cp_2Fe^+. In contrast to the behavior of the complexes $[(Me_3tacn)MoX_3]$ (X = Cl, Br, I) in acetonitrile,[12] no reversible oxidation event is apparent. The effective moment of **2** at room temperature was measured as 3.59 μ_B, which is slightly below the spin-only value for an $S = 3/2$ species and indicates a g factor of 1.85. This result differs somewhat from the magnetic properties observed for Mo^{III} in the presence of a more rigorously octahedral ligand field, such as in $[MoCl_6]^{3-}$ ($g = 1.93$) and $[Mo(H_2O)_6]^{3+}$ ($g = 1.95$).[26] Further investigation of complex **2** using high-field EPR spectroscopy is underway, in an effort to determine both the sign and magnitude of its zero-field splitting parameter D.[27]

Upon exposure to air, **2** and **3** are stable for several months as solids, but gradually decompose over the course of several days in solution. In both cases, $[(Me_3tacn)MoO(CN)_2]$ (**4**) is prominent among the initial oxidation products. This six-coordinate Mo^{IV} species is recognizable by its pale blue color and crystallizes from aqueous solution as **4**·H_2O. Two independent complexes are present in the crystal structure, and one of these is depicted in Figure 1c; relevant mean interatomic distances and angles are listed in Table 1. The short Mo−O distances of 1.741(5) and 1.687(4) Å are consistent with the expected double-bond character and result in longer trans Mo−N distances of 2.397(5) and 2.410(5) Å, respectively. In all, the structure is quite comparable to that of $[(Me_3tacn)MoOI_2]$.[28]

Face-Centered Cubic $Mo_8Ni_6(CN)_{24}$. In an exact parallel of eq 1, $[(Me_3tacn)Mo(CN)_3]$ reacts with nickel(II) bromide in boiling aqueous solution to give $[(Me_3tacn)_8Mo_8Ni_6(CN)_{24}]Br_{12}\cdot 27H_2O$ (**6**).

$$8[(Me_3tacn)Mo(CN)_3] + 6[Ni(H_2O)_6]^{2+} \rightarrow [(Me_3tacn)_8Mo_8Ni_6(CN)_{24}]^{12+} \quad (4)$$

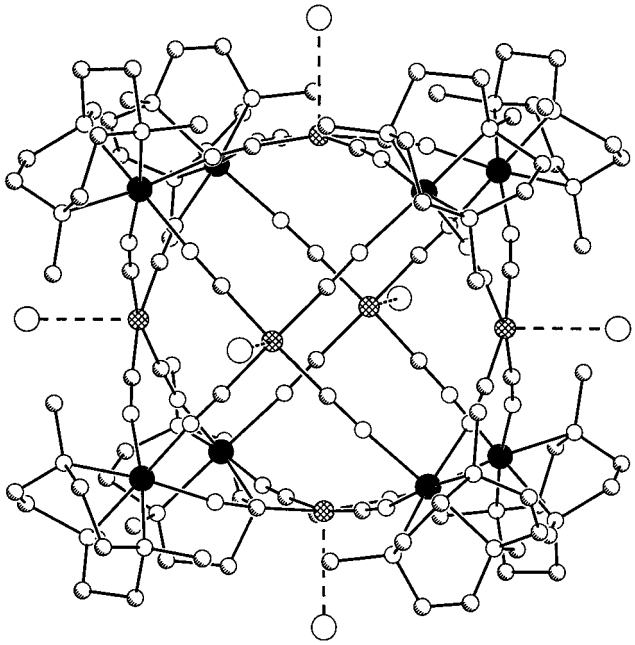

Figure 3. Structure of the face-centered cubic $[(Me_3tacn)_8Mo_8Ni_6(CN)_{24}]^{12+}$ cluster in **6**·$3H_2O$. H atoms are omitted for clarity. Black, crosshatched, shaded, small white, and large white spheres represent Mo, Ni, C, N, and Br atoms, respectively. The cluster resides on a $\bar{3}$ symmetry site in the crystal.

Table 2. Selected Mean Interatomic Distances (Å) and Angles (deg) for the Face-Centered Cubic $[(Me_3tacn)_8M_8Ni_6(CN)_{24}]^{12+}$ (M = Cr, Mo) Clusters in the Structures of $[(Me_3tacn)_8Cr_8Ni_6(CN)_{24}]Br_{12}\cdot 45H_2O$,[5b] $[(Me_3tacn)_8Mo_8Ni_6(CN)_{24}]Br_{12}\cdot 30H_2O$ (**6**·$3H_2O$), and $[(Me_3tacn)_8Mo_8Ni_6(CN)_{24}]I_{12}\cdot 27H_2O$ (**7**·$9H_2O$)[a]

	M = Cr	**6**·$3H_2O$	**7**·$9H_2O$
$M-N_{CN}$	2.031(7)	2.126(6)	2.10(2)
Ni−C	1.873(9)	1.86(1)	1.883(5)
$C-N_{CN}$	1.145(6)	1.15(2)	1.14(2)
$M-N_{tacn}$	2.066(5)	2.175(8)	2.181(8)
M···Ni	5.019(2)	5.114(2)	5.10(1)
M···M	6.97(2)	7.07(5)	7.06(3)
trans-Ni···Ni	8.844	9.177	9.186
Ni···X[b]	2.802	2.797	2.900
$N_{CN}-M-N_{CN}$	88.0(3)	88.3(3)	88.7(7)
$M-N_{CN}-C$	169.1(5)	170.6(8)	171(1)
C−Ni−C	89.6(3)	89.5(4)	89.3(4)
	170.0(5)	168.6(1)	167(1)
Ni−C−N	177(2)	176.1(9)	177(1)
$N_{CN}-M-N_{tacn}$	94.4(2)	95.3(2)	95.5(5)
	176.6(3)	174.3(2)	174.1(3)
$N_{tacn}-M-N_{tacn}$	83.0(1)	80.4(2)	80.0(3)

[a] N_{CN} and N_{tacn} indicate N atoms in cyanide and Me_3tacn ligands, respectively. [b] X = Br or I.

Single crystals of **6**·$3H_2O$ were obtained by allowing an aqueous solution of the product to slowly evaporate, and X-ray analysis revealed the compound to be isostructural with $[(Me_3tacn)_8Cr_8Ni_6(CN)_{24}]Br_{12}\cdot 45H_2O$.[5b] Figure 3 depicts the structure of the $[(Me_3tacn)_8Mo_8Ni_6(CN)_{24}]^{12+}$ cluster, which features a tightly connected metal−cyanide cage with eight Mo^{III} ions positioned at the corners of a cube and six Ni^{II} ions situated slightly above each cube face. An outer bromide anion forms a weak axial interaction with each square-planar nickel center, and ignoring Me_3tacn conformations, the cluster closely conforms to its maximal point group symmetry of O_h. Table 2 provides a list of mean interatomic distances and angles, along with those of

(26) (a) Bowers, K. D.; Owen, J. *Rep. Prog. Phys.* **1955**, *18*, 304. (b) Jacobsen, C. J. H.; Pedersen, E. *Inorg. Chem.* **1991**, *30*, 4477.
(27) Sokol, J. J.; Saylor, C.; Shores, M. P.; Brunel, L.-C.; Long, J. R. Work in progress.
(28) Bürger, K. S.; Haselhorst, G.; Stötzel, S.; Weyhermüller, T.; Wieghardt, K.; Nuber, B. *J. Chem. Soc., Dalton Trans.* **1993**, 1987.

$[(Me_3tacn)_8Cr_8Ni_6(CN)_{24}]^{12+}$ for comparison. The chief geometric differences between the two clusters are a consequence of the larger size of Mo^{III}, which leads to an overall expansion of the face-centered cubic cage. The expansion is perhaps most obvious in the increase of the trans-Ni···Ni distances from 8.844 to 9.177 Å, which inflates the internal cavity to a minimum diameter of 6.0 Å (based on the van der Waals radius of nickel).[29] As observed in the analogous chromium-containing clusters,[5b] this cavity appears to be empty: no build-up of electron density attributable to guest water molecules is evident in the crystal structure, and no water molecules are associated with peaks corresponding to the intact cluster in the electrospray mass spectrum. Note that access in and out of the cavity is severely hindered by the methyl groups of the Me_3tacn ligands.[30] Interestingly, the reaction between $[(Me_3tacn)Mo(CN)_3]$ and NiI_2 in aqueous solution produces the $[(Me_3tacn)_8Mo_8Ni_6(CN)_{24}]I_{12}\cdot 18H_2O$ (**7**), the iodide salt of the same cluster. In contrast, the analogous reaction employing $[(Me_3tacn)Cr(CN)_3]$ affords $[(Me_3tacn)_8Cr_8Ni_5(CN)_{24}]I_{10}\cdot 27H_2O$, wherein a Ni^{II} center is missing from the cluster cage and an iodide anion is trapped inside the cavity.[5c] The crystal structure of $\mathbf{7}\cdot 9H_2O$ reveals no significant differences from the geometry observed in the bromide salt of the cluster (see Table 2).

Inherent to the formation of $[(Me_3tacn)_8Mo_8Ni_6(CN)_{24}]^{12+}$ is a thermally induced linkage isomerization, in which the cyanide ligands reorient to give a $Mo^{III}-N-C-Ni^{II}$ connectivity. This type of isomerization also occurs during formation of the analogous chromium-containing cluster[5b] and has long been known to occur in certain Prussian blue analogues.[31] The process is driven by thermodynamics, with the softer carbon end of cyanide preferring to bind the softer Ni^{II} ion. Ligation by the stronger field end of cyanide then causes the nickel centers to adopt a square-planar coordination geometry and a diamagnetic electron configuration. Indeed, the core structure of $[(Me_3tacn)_8Mo_8Ni_6(CN)_{24}]^{12+}$ can be viewed as containing six slightly bowed square-planar $[Ni(CN)_4]^{2-}$ units capping the faces of an Mo_8 cube. Of course, the loss of unpaired electrons at the nickel sites has a dramatic impact on the magnetic behavior of **6** (see Figure S2 in the Supporting Information). At 295 K, the value of $\chi_M T$ is 14.34 cm^3 K/mol, slightly below the spin-only value of 15.00 cm^3 K/mol expected for eight uncoupled $S = 3/2$ metal ions. The low $\chi_M T$ value indicates a g factor of 1.956, which is higher than that observed for $[(Me_3tacn)Mo(CN)_3]$. As the temperature is lowered, $\chi_M T$ remains constant down to approximately 50 K, whereafter it begins to decrease, reaching a value of 7.14 cm^3 K/mol at 2.0 K. Analogous to the situation in $[(Me_3tacn)_8Cr_8Ni_6(CN)_{24}]^{12+}$,[5b] the decrease in $\chi_M T$ is attributed to weak antiferromagnetic interactions between Mo^{III} centers through the LUMO orbitals of the intervening $[Ni(CN)_4]^{2-}$ units. The fact that the decrease becomes apparent at a higher temperature for the molybdenum-containing cluster is consistent with a slightly stronger exchange interaction, as might be anticipated for the more diffuse valence *d* orbitals. This issue is obscured somewhat, however, by the possible contributions from zero-field splitting.

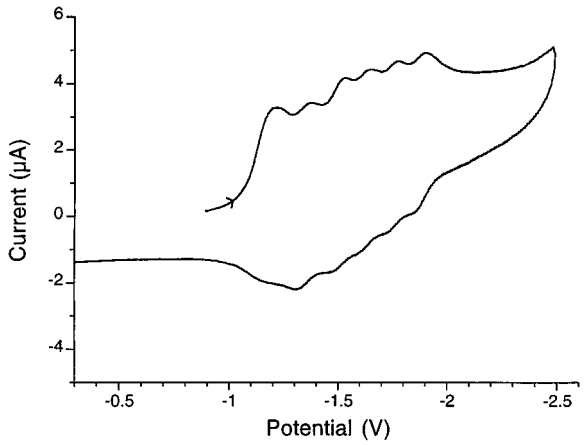

Figure 4. Cyclic voltammogram of $[(Me_3tacn)_8Mo_8Ni_6(CN)_{24}]Br_{12}\cdot 27H_2O$ (**6**) in DMF. Potentials are reported relative to Cp_2Fe/Cp_2Fe^+. As the potential becomes more reducing, peaks occur at −1.240, −1.434, −1.516, −1.660, −1.783, and −1.910 V, whereas, in the return scan, peaks occur at −1.843, −1.720, −1.587, −1.492, −1.318, and −1.158 V.

Carrying out the analogous reaction with $[(Me_3tacn)Cr(CN)_3]$ (eq 1) in methanol at −40 °C permits isolation of a green metastable precursor to the $[(Me_3tacn)_8Cr_8Ni_6(CN)_{24}]^{12+}$ cluster, which was found to display magnetic properties consistent with an $S = 18$ ground state.[5b] Although this high-spin species could not be crystallized at low temperature, it is thought to possess the same face-centered cubic cage topology, albeit with paramagnetic nickel centers and $Cr^{III}-C-N-Ni^{II}$ bridges leading to ferromagnetic coupling. Upon warming to room temperature, the cyanide ligands gradually isomerize (as monitored by infrared spectroscopy), and the ferromagnetic coupling is destroyed. Our initial expectation was that by replacing the Cr^{III} ions in the cluster with softer Mo^{III} ions, the driving force for linkage isomerization would be reduced substantially, possibly enabling us to crystallize the high-spin form of the cluster. While the reaction between $[(Me_3tacn)Mo(CN)_3]$ and nickel(II) bromide at −40 °C in methanol indeed produces a green metastable precursor, its subsequent conversion to the low-spin cyanide-isomerized product is actually much more rapid. At room temperature, infrared spectra show the transformation of the green solid into orange compound **6** to be essentially complete after just five minutes. Thus, it appears that substituting Mo^{III} for Cr^{III} may lower the activation barrier for the linkage isomerization reaction. Presumably, this too occurs as a consequence of the more diffuse valence *d* orbitals of Mo^{III}, which help stabilize the side-bound cyanide unit in the putative $Mo^{III}-(\eta^2{:}\eta^2\text{-CN})-Ni^{II}$ transition state.

With Mo^{III} replacing Cr^{III}, the new $[(Me_3tacn)_8Mo_8Ni_6(CN)_{24}]^{12+}$ cluster exhibits some unusual redox chemistry. The reduction event observed at $E_{1/2} = -1.895$ V for the $[(Me_3tacn)Mo(CN)_3]$ complex (see Figure S1 in the Supporting Information) is manifested as a sequence of six closely spaced reduction waves in the cyclic voltammagram of cluster compound **6** in DMF. As shown in Figure 4, the waves all occur at less negative potentials, with $E_{1/2} = -1.199$ V ($\Delta E_p = 82$ mV), −1.376 V ($\Delta E_p = 128$ mV), −1.504 V ($\Delta E_p = 24$ mV), −1.624 V ($\Delta E_p = 73$ mV), −1.752 V ($\Delta E_p = 63$ mV), and −1.877 V ($\Delta E_p = 67$ mV) versus Cp_2Fe/Cp_2Fe^+. Thus, each electron

(29) Bondi, A. *J. Phys. Chem.* **1964**, *68*, 441.
(30) Pertinently, water is also not observed inside the cavity of an analogous $[(tach)_8Cr_8Ni_6(CN)_{24}]^{12+}$ (tach = 1,3,5-triaminocyclohexane) cluster featuring less sterically demanding outer ligands: Yang, J. Y.; Shores, M. P.; Sokol, J. S.; Long, J. R., manuscript in preparation.
(31) (a) Shriver, D. F.; Shriver, S. A.; Anderson, S. E. *Inorg. Chem.* **1965**, *4*, 725. (b) Brown, D. B.; Shriver, D. F.; Schwartz, L. H. *Inorg. Chem.* **1968**, *7*, 77. (c) Brown, D. B.; Shriver, D. F. *Inorg. Chem.* **1969**, *8*, 37. (d) House, J. E., Jr.; Bailar, J. C., Jr. *Inorg. Chem.* **1969**, *8*, 672. (e) Reguera, E.; Bertrán, J. F.; Nuñez, L. *Polyhedron* **1994**, *13*, 1619.

added to the cluster is noticeably affected by the presence of any previously added electrons. The separations between successive reduction waves indicate comproportionation constants falling in the range $K_c = 100-1000$, consistent with class II mixed-valence behavior.[32] Similar to the situation in Prussian blue,[33] electron delocalization in a mixed-valence Mo^{II}/Mo^{III} redox state of the cluster may therefore be expected to give rise to ferromagnetic coupling via a double-exchange mechanism. Accordingly, the one-electron reduced cluster $[(Me_3tacn)_8Mo_8Ni_6(CN)_{24}]^{11+}$ is predicted to have an $S = 23/2$ ground state. Efforts to produce such reduced forms of the cluster via titration of an appropriate reductant are underway.

Linear $NiMo_2(CN)_6$. Ultimately, we envision using trans-directing cyclam complexes in combination with tacn-ligated corner units to assemble edge-bridged cubic clusters of the type $[(tacn)_8(cyclam)_{12}M_{12}M'_8(CN)_{24}]^{x+}$. As yet, reactions targeting such a species—including efforts employing $[(Me_3tacn)Mo(CN)_3]$—have either failed to give the desired product or have not led to single crystals suitable for a complete X-ray analysis. However, certain of these attempts have been found to follow the course of eq 2 above, resulting in isolation and structural characterization of $[(Me_3tacn)_2(cyclam)NiCr_2(CN)_6]^{2+}$, a linear cluster consisting of a single edge fragment of the larger 20-metal species.[5b] In close parallel, reactions between $[(Me_3tacn)Mo(CN)_3]$ and the bromide, iodide, and perchlorate salts of $[(cyclam)Ni(H_2O)_2]^{2+}$ afford linear $[(Me_3tacn)_2(cyclam)NiMo_2(CN)_6]^{2+}$ clusters, as observed in **9**−**11**.

$$2[(Me_3tacn)Mo(CN)_3] + [(cyclam)Ni(H_2O)_2]^{2+} \rightarrow [(Me_3tacn)_2(cyclam)NiMo_2(CN)_6]^{2+} \quad (5)$$

The compounds are isolated cleanly by employing the 2:1 Mo:Ni stoichiometry of eq 5, and are stable in air in the solid state. Interestingly, the influence of the counteranions and solvate molecules on the crystal structure of the product can play a significant role in determining its magnetic properties.

Conducting eq 5 with $[(cyclam)NiI_2]$ in acetonitrile instead of water produces $[\alpha\text{-}(Me_3tacn)_2(cyclam)NiMo_2(CN)_6]I_2$ (**8**) in high yield. As crystallized from DMF, this compound features the usual linear cluster connectivity, wherein two $[(Me_3tacn)Mo(CN)_3]$ complexes coordinate a central $[(cyclam)Ni]^{2+}$ unit in a trans geometry (see Figure 5, upper). The cluster resides on an inversion center, such that, with respect to its approximately linear $[Mo-CN-Ni-NC-Mo]^{6+}$ core, the two Me_3tacn ligands are disposed in an anti conformation (here denoted as the α isomer). The minimum C−Mo···Mo−C torsion angle of 90.6° provides a quantitative measure of the conformation, which, not surprisingly, can be influenced appreciably by crystal packing forces. For example, the crystal structure of $[(Me_3tacn)_2(cyclam)NiCr_2(CN)_6](ClO_4)_2\cdot 2H_2O$[5b] features an analogous cluster, wherein the Me_3tacn ligands are twisted toward each other to give a minimum C−Cr···Cr−C torsion angle of 34.1°. Selected mean interatomic distances and angles from the two structures are compared in Table 3. Aside from the usual differences arising from the larger size of Mo^{III}, the most noteworthy distinction between the two cluster geometries lies in the $Ni-N_{CN}-C$ angles, which are more linear in the conformation adopted by the chromium-containing species.

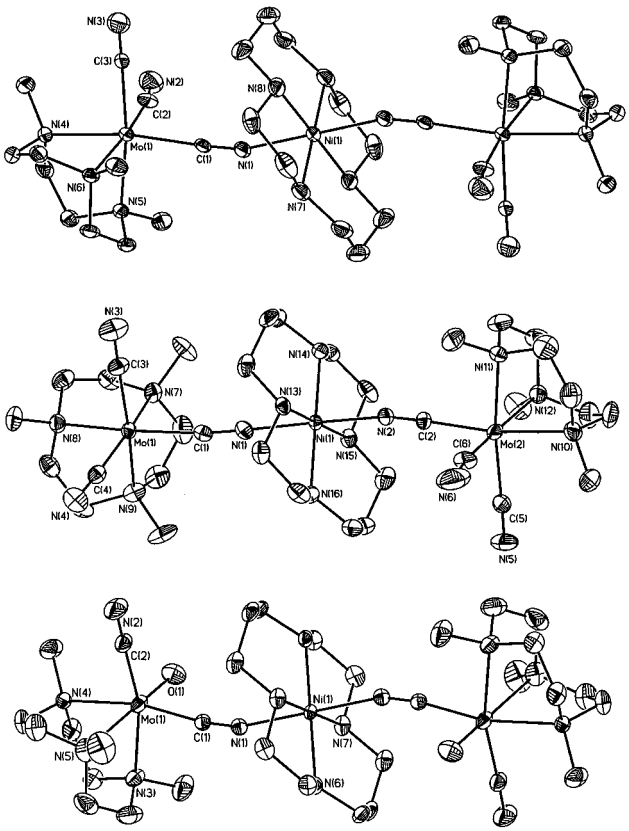

Figure 5. Structure of the linear clusters $[\alpha\text{-}(Me_3tacn)_2(cyclam)NiMo_2(CN)_6]^{2+}$ in **8**·2DMF (upper), $[\beta\text{-}(Me_3tacn)_2(cyclam)NiMo_2(CN)_6]^{2+}$ in **11** (middle), and $[(Me_3tacn)_2(cyclam)Ni-Mo_2(O)_2(CN)_4]^{2+}$ in **12** (lower), showing 40% probability ellipsoids. H atoms are omitted for clarity. The upper and lower clusters reside on crystallographic inversion centers. Selected interatomic distances (Å) and angles (°) from the structure of **12**: Mo(1)−C(1) 2.163(7), Mo(1)−C(2) 2.152(7), Mo(1)−O(1) 1.754(5), Ni(1)−N(1) 2.127(5), C(1)−N(1) 1.145(8), C(2)−N(2) 1.156(9), Mo(1)−N(3) 2.238(5), Mo(1)−N(4) 2.255(5), Mo(1)−N(5) 2.387(7), Ni(1)−N(6) 2.087(5), Ni(1)−N(7) 2.091(5), C(1)−Mo(1)−C(2) 88.6(2), C(1)−Mo(1)−O(1) 95.2(3), C(2)−Mo(1)−O(1) 100.0(3), Mo(1)−C(1)−N(1) 171.4(6), Mo(1)−C(2)−N(2) 178.2(7), Ni(1)−N(1)−C(1) 161.8(5), N(3)−Mo(1)−C(1) 94.2(2), N(4)−Mo(1)−C(1) 165.1(2), N(5)−Mo(1)−C(1) 89.9(2), N(6)−Ni(1)−N(1) 89.8(2), N(7)−Ni(1)−N(1) 89.8(2), N(6)−Ni(1)−N(7) 94.4(2).

Substitution of Mo^{III} for Cr^{III} in the linear $NiM_2(CN)_6$ cluster motif leads to stronger magnetic exchange coupling and increased magnetic anisotropy. The magnetic properties of $[(Me_3tacn)_2(cyclam)NiCr_2(CN)_6](ClO_4)_2\cdot 2H_2O$ are consistent with an $S = 4$ ground state stemming from the predicted[8] ferromagnetic coupling between the Cr^{III} (t_{2g}^3) and Ni^{II} ($t_{2g}^6e_g^2$) centers.[5b] A fit to the susceptibility data gave $g = 2.00$ and an exchange coupling constant of $J = 10.9$ cm^{-1}, whereas the magnetization behavior showed no appreciable zero-field splitting.[5b] In contrast, zero-field splitting *is* evident in the magnetization data obtained for $[\alpha\text{-}(Me_3tacn)_2(cyclam)NiMo_2(CN)_6]I_2$ (**8**), as recognizable in Figure 6 from the downturn of the curves with increasing H/T. Assuming an $S = 4$ ground state and negligible population of excited states at the temperatures probed, the data were fit using ANISOFIT to give zero-field splitting parameters of $D = 0.44$ cm^{-1} and $E = 0.13$ cm^{-1} with $g = 1.81$. Note that the sign of D is not reliably established

(32) (a) Robin, M. B.; Day, P. *Adv. Inorg. Chem. Radiochem.* **1967**, *10*, 247. (b) Richardson, D. E.; Taube, H. *Inorg. Chem.* **1981**, *20*, 1278. (c) Creutz, C. *Prog. Inorg. Chem.* **1983**, *30*, 1. (d) Kaim, W.; Klein, A.; Glöckle, M. *Acc. Chem. Res.* **2000**, *33*, 755.

(33) Mayoh, B.; Day, P. *J. Chem. Soc., Dalton Trans.* **1976**, 1483.

Table 3. Selected Mean Interatomic Distances (Å) and Angles (deg) for the Linear $[(Me_3tacn)_2(cyclam)NiM_2(CN)_6]^{2+}$ (M = Cr, Mo) Clusters in the Structures of $[(Me_3tacn)_2(cyclam)NiCr_2(CN)_6](ClO_4)_2\cdot 2H_2O$,[5b] $[\alpha\text{-}(Me_3tacn)_2(cyclam)NiMo_2(CN)_6]I_2\cdot 2DMF$ (**8**·2DMF), $[\beta\text{-}(Me_3tacn)_2(cyclam)NiMo_2(CN)_6]I_2\cdot 7H_2O$ (**9**·H_2O), $[\alpha\text{-}(Me_3tacn)_2(cyclam)NiMo_2(CN)_6]Br_2\cdot 6H_2O$ (**10**), and $[\beta\text{-}(Me_3tacn)_2(cyclam)NiMo_2(CN)_6](ClO_4)_2\cdot 2H_2O$ (**11**)[a]

	M = Cr	**8**·2DMF	**9**·H_2O	**10**	**11**
M−C	2.068(9)	2.16(2)	2.14(2)	2.13(2)	2.10(8)
Ni−N_{CN}	2.108(8)	2.152(3)	2.107(7)	2.106(3)	2.113(7)
C−N_{CN}	1.15(1)	1.12(3)	1.16(2)	1.17(3)	1.15(2)
M−N	2.107(3)	2.237(5)	2.233(3)	2.232(9)	2.22(2)
Ni−N_{cyclam}	2.072(3)	2.068(7)	2.078(6)	2.077(6)	2.052(6)
C−M−C	89(2)	93(4)	89(2)	91(1)	92(3)
M−C−N_{CN}	176(2)	174(4)	176(3)	176.0(5)	176(3)
N_{CN}−Ni−N_{CN}	177.4(1)	180	179.6(4)	180	177.5(2)
Ni−N_{CN}−C	170(1)	163.6(3)	171.1(7)	164.8(3)	172(4)
N−M−C	94(2)	93(2)	95.4(9)	95(2)	94(2)
	175(1)	171(2)	173(1)	172(2)	170.9(8)
N−M−N	83.6(3)	79.6(2)	79.5(3)	79.3(2)	79.2(7)
N_{cyclam}−Ni−N_{CN}	90(1)	90(1)	90(1)	90.0(7)	90(1)
N_{cyclam}−Ni−N_{cyclam}	85.2(6)	85.9(2)	85.4(1)	86.0(1)	85.2(5)
	94.8(6)	94.1(2)	94.6(3)	94.1(1)	94.9(5)
minimum C−M···M−C	34.1	90.6	16.7	87.5	11.4

[a] N_{CN} and N_{cyclam} indicate N atoms in cyanide and cyclam ligands, respectively.

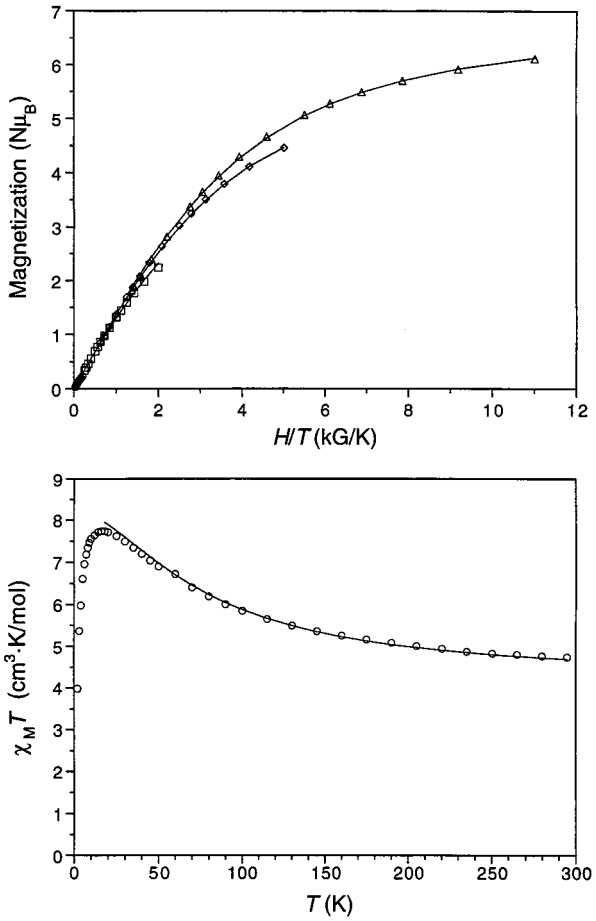

Figure 6. Magnetic behavior of $[\alpha\text{-}(Me_3tacn)_2(cyclam)NiMo_2(CN)_6]I_2$ (**8**). Data represented by circles, squares, diamonds, and triangles were measured in an applied field of 1, 10, 25, and 55 kG, respectively. Solid lines represent calculated fits to the data; see text for details.

from such powder measurements;[34] generally, a comparable fit with the opposite sign for D can also be obtained. The variation of $\chi_M T$ with temperature observed for **8** is plotted in Figure 6. At room temperature, it lies very near the spin-only value of 4.75 cm^3 K/mol expected for one $S = 1$ and two $S = 3/2$ ions in the absence of magnetic coupling. Consistent with ferromagnetic coupling, $\chi_M T$ rises monotonically with decreasing temperature before reaching a maximum of 7.74 cm^3 K/mol at 16 K. The subsequent drop as the temperature continues to decrease is attributed to zero-field splitting. Figure 6 shows the best fit to the data above 16 K, which was obtained using MAGFIT 3.1 with a single pairwise exchange parameter and an exchange Hamiltonian of the following form.

$$\hat{H} = -2J[\hat{S}_{Ni}\cdot(\hat{S}_{Mo(1)} + \hat{S}_{Mo(2)})] \qquad (6)$$

This fit gives $g = 1.80$ and a coupling constant of $J = 17.6$ cm^{-1}. Thus, replacing Cr^{III} with Mo^{III} in the cluster appears to increase the strength of the magnetic exchange coupling by as much as 60%. Significantly, including a second exchange parameter in eq 6 to account for long-range coupling between the two molybdenum centers did not improve the fit and did not reproduce the drop in $\chi_M T$ at lower temperatures.

The iodide salt of $[(Me_3tacn)_2(cyclam)NiMo_2(CN)_6]^{2+}$ crystallizes from water as $[\beta\text{-}(Me_3tacn)_2(cyclam)NiMo_2(CN)_6]I_2\cdot 7H_2O$ (**9**·H_2O), featuring a different conformation of the linear cluster. The geometry of this β isomer approximates that depicted in the middle of Figure 5 and differs from the α isomer observed in **8**·2DMF (Figure 5, upper) by virtue of having its Me_3tacn ligands twisted away from the anti configuration. The extent of the twist is such that two of the cyanide ligands are oriented in essentially the same direction, resulting in a minimum C−Mo···Mo−C torsion angle of 16.7°. Accordingly, the conformation of the β isomer is closer to that of the chromium-containing cluster in $[(Me_3tacn)_2(cyclam)NiCr_2(CN)_6](ClO_4)_2\cdot 2H_2O$,[5b] and it exhibits more linear Ni−N_{CN}−C angles than the α isomer (see Table 3). The magnetic behavior of **9** differs from that of **8** primarily in the magnitude of the zero-field splitting parameters. The best fit to the magnetization data gives $g = 1.77$, $D = -0.56$ cm^{-1}, and $E = 0.0029$ cm^{-1}, while using the exchange Hamiltonian in eq 6, the best fit to the susceptibility data at $T \geq 14$ K gives $g = 1.80$ and $J = 17.0$ cm^{-1}.[35] Interestingly, the behavior of $[\alpha\text{-}(Me_3tacn)_2(cyclam)NiMo_2(CN)_6]Br_2\cdot 6H_2O$ (**10**) is very similar, with the best fit to the magnetization data yielding $g = 1.80$, $D = -0.72$ cm^{-1}, and $E = -0.055$ cm^{-1}, and the best fit to the susceptibility data ($T \geq 12$ K) indicating $g = 1.83$ and $J = 17.3$ cm^{-1}.[35] Thus, it seems that, despite altering the Ni−N_{CN}−C angles, the different cluster conformations have little effect on the strength of the magnetic exchange coupling. The conformation does, however, appear to have an influence on the magnetic anisotropy. If the sign and magnitude of these D values are correct, then **9** and **10** can be anticipated to behave as single-molecule magnets with spin reversal barriers of 9 and 12 cm^{-1}, respectively.

Quite distinct magnetic behavior is observed for the perchlorate salt of the linear cluster, which crystallizes from aqueous solution as $[\beta\text{-}(Me_3tacn)_2(cyclam)NiMo_2(CN)_6](ClO_4)_2\cdot 2H_2O$ (**11**). With a minimum C−Mo···Mo−C torsion angle of 11.4°, the conformation adopted by the cluster in this compound

(34) Kahn, O. *Molecular Magnetism*; VCH: New York, 1993.

(35) Figures showing these data together with the corresponding fits are presented in the Supporting Information.

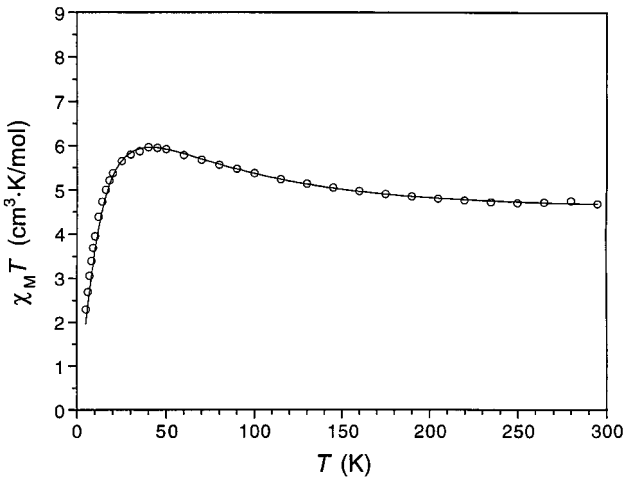

Figure 7. Magnetic behavior of [β-$(Me_3tacn)_2$(cyclam)$NiMo_2(CN)_6$]$(ClO_4)_2$·$2H_2O$ (**11**), as measured at 1000 G. The solid line represents the calculated fit to the data.

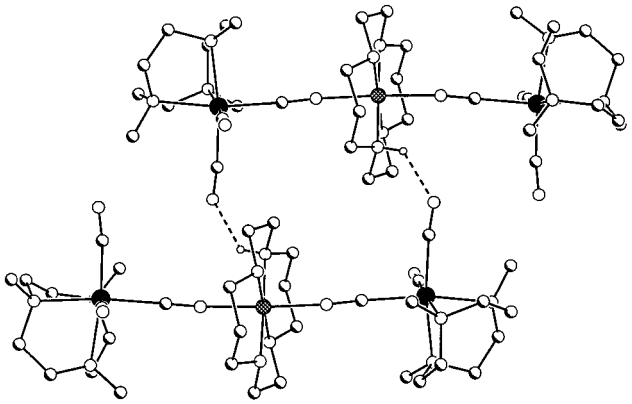

Figure 8. Hydrogen-bonding interactions between two linear clusters in the structure of [β-$(Me_3tacn)_2$(cyclam)$NiMo_2(CN)_6$]$(ClO_4)_2$·$1.5H_2O$ (**11**). Black, crosshatched, shaded, large white, and small white spheres represent Mo, Ni, C, N, and H atoms, respectively. For clarity, only the H atoms involved in forming the postulated Mo−C−N···H−N−Ni exchange pathways are depicted. Associated with this pathway are the interatomic distances (Å): N···H 2.449, N···N 3.144, Mo···Ni 7.197. The two clusters are related by an inversion center in the crystal.

(Figure 5, middle) closely resembles that in the structure of **9**·H_2O. However, as shown in Figure 7, the magnetic susceptibility data for **11** differ considerably from the results obtained for **8**−**10**. Although the value of $\chi_M T$ at room temperature is nearly identical for all four compounds, its steady rise with decreasing temperature is heavily attenuated in **11**: a lower maximum value of 5.96 cm^{3}K/mol is achieved at the higher temperature of 40 K. The origin of this difference likely traces to the crystal structure of **11**, which is the only one to display hydrogen bonding contacts directly between cluster units. Here, somewhat long hydrogen bonds between a N−H group of a cyclam ligand in one cluster and a terminal cyanide ligand in another serve to pair the clusters up into dimers, as illustrated in Figure 8. By assuming that the resultant Mo−C−N···H−N−Ni connections provide a second pathway for magnetic superexchange, the following exchange Hamiltonian was used to generate a fit to the susceptibility data.

$$\hat{H} = -2\{J[\hat{S}_{Ni(1)}\cdot(\hat{S}_{Mo(1)} + \hat{S}_{Mo(2)}) + \hat{S}_{Ni(2)}\cdot(\hat{S}_{Mo(3)} + \hat{S}_{Mo(4)})] + J'(\hat{S}_{Ni(1)}\cdot\hat{S}_{Mo(3)} + \hat{S}_{Ni(2)}\cdot\hat{S}_{Mo(2)})\} \quad (7)$$

Neglecting any contribution from zero-field splitting, the fit matches the data well (see Figure 7) and gives $g = 1.79$, $J = 14.9$ cm^{-1}, and $J' = -1.9$ cm^{-1}. Hence, the ferromagnetic coupling between Mo^{III} and Ni^{II} centers within the cluster appears to be slightly diminished relative to that in **8**−**10**, and the reduction in $\chi_M T$ at low temperatures is attributed to the weak antiferromagnetic coupling between Mo^{III} and Ni^{II} centers situated in neighboring clusters. Hydrogen-bonded pathways have been invoked to account for long-range magnetic ordering in other metal−cyanide compounds,[6h,36] but, to our knowledge, this type of supramolecular pairing has not previously been observed.

If, in the course of preparing [$(Me_3tacn)_2$(cyclam)$NiMo_2$-$(CN)_6]^{2+}$, the reaction solution is allowed to stand in air for an extended period, partial oxidation of [$(Me_3tacn)Mo(CN)_3$] occurs, leading to contamination of the product with [$(Me_3tacn)_2$-(cyclam)$NiMo_2(O)_2(CN)_4]^{2+}$. Formation of this oxidized species is facilitated by using an excess of [(cyclam)$Ni(H_2O)_2]^{2+}$, which potentially aids in the release of cyanide from the molybdenum complex. As crystallized in [$(Me_3tacn)_2$(cyclam)$NiMo_2(O)_2$-$(CN)_4]I_2$·$6H_2O$ (**12**), its structure consists of the usual linear cluster arrangement, albeit with one terminal cyanide ligand on each molybdenum center replaced by an oxo group (see Figure 5, lower). The conformation of the cluster is comparable to that adopted by the α isomer of the $NiMo_2(CN)_6$ cluster in **8**·2DMF (Figure 5, upper). Selected interatomic distances and angles are listed in the legend of Figure 5; overall, the coordination geometry of the Mo^{IV} centers is similar to that found in [$(Me_3$-tacn)Mo(O)$(CN)_2$] (see Table 1). The magnetic properties of **12** have not yet been investigated.

Zigzag $Ni_3Mo_2(CN)_6$. The presence of terminal cyanide ligands in the linear [$(Me_3tacn)_2$(cyclam)$NiMo_2(CN)_6]^{2+}$ cluster suggests the possibility of utilizing it as a platform for attaching additional magnetically coupled metal ions. Unfortunately, however, infrared spectra indicate that the cluster dissociates upon dissolution. Nonetheless, such constructs can be realized by increasing the number of equivalents of [(cyclam)Ni-$(H_2O)_2]^{2+}$ employed in eq 5. With bromide as a counterion, using a large excess of the nickel complex in aqueous solution prompts formation of a five-metal species, in accord with the following reaction.

$$2[(Me_3tacn)Mo(CN)_3] + 3[(cyclam)Ni(H_2O)_2]^{2+} \rightarrow [(Me_3tacn)_2(cyclam)_3(H_2O)_2Ni_3Mo_2(CN)_6]^{6+} \quad (8)$$

Approximately an extra 7 equiv of [(cyclam)$Ni(H_2O)_2]^{2+}$ is required to obtain [$(Me_3tacn)_2(cyclam)_3(H_2O)_2Ni_3Mo_2(CN)_6]Br_6$·$9H_2O$ (**13**) as the only molybdenum-containing product. Reducing the reaction solution to dryness affords an intimate mixture of **13** and [(cyclam)$NiBr_2$], which, owing to their solubility properties, are not readily separated. Prior to drying, crystals of **13**·$5H_2O$ are present in the mixture. An X-ray analysis revealed the zigzag cluster depicted at the top of Figure 9,

(36) (a) Ferlay, S.; Mallah, T.; Vaissermann, J.; Bartolomé, F.; Veillet, P.; Verdaguer, M. *Chem. Commun.* **1996**, 2481. (b) Kou, H.-Z.; Liao, D.-Z.; Cheng, P.; Jiang, Z.-H.; Yan, S.-P.; Wang, G.-L.; Yao, X.-K.; Wang, H.-G. *J. Chem. Soc., Dalton Trans.* **1997**, 1503. (c) Van Langenberg, K.; Batten, S. R.; Berry, K. J.; Hockless, D. C. R.; Moubaraki, B.; Murray, K. S. *Inorg. Chem.* **1997**, *36*, 5006. (d) Marvilliers, A.; Parsons, S.; Rivière, E.; Audière, J.-P.; Mallah, T. *Chem. Commun.* **1999**, 2217. (e) Yan, B.; Wang, S.; Chen, Z. *Monatsh. Chem.* **2001**, *132*, 305.

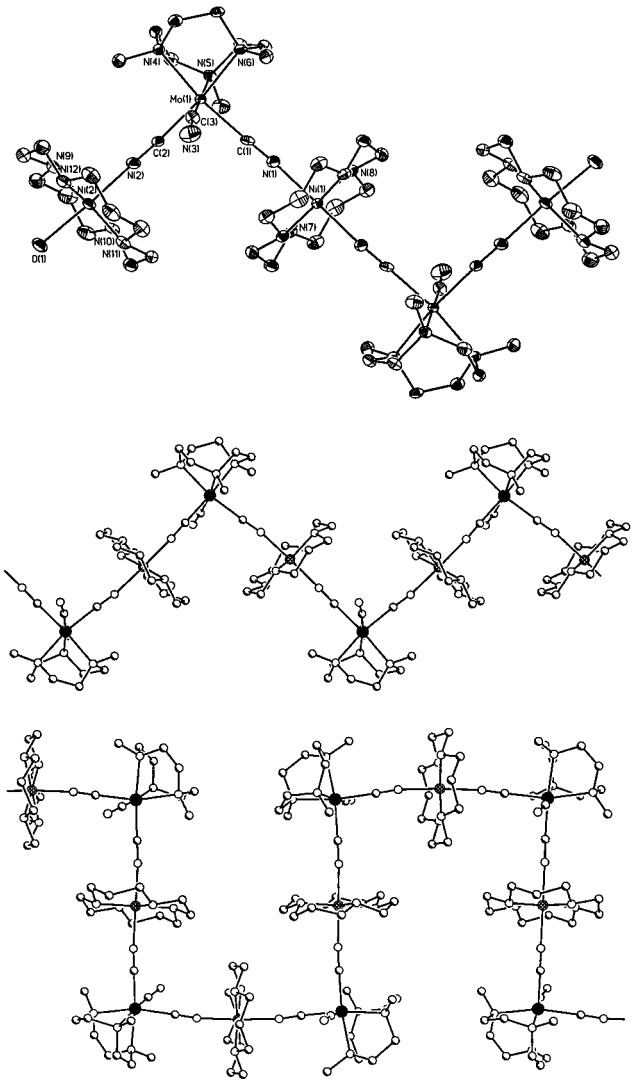

Figure 9. (Upper) Structure of the zigzag $[(Me_3tacn)_2(cyclam)_3(H_2O)_2Ni_3Mo_2(CN)_6]^{6+}$ cluster in **13**·$5H_2O$, showing 40% probability ellipsoids. H atoms are omitted for clarity. The molecule resides on an inversion center in the crystal. Selected mean interatomic distances (Å) and angles (°): Mo−C 2.13(5), Ni−N_{CN} 2.103(8), C−N_{CN} 1.17(3), Mo−N 2.24(1), Ni−N_{cyclam} 2.072(3), Ni−O 2.221, C−Mo−C 90(3), Mo−C−N 172(3), Ni−N_{CN}−C 173(3), N−Mo−C 95(2), 173(3), N−Mo−N 79.7(3), N_{cyclam}−Ni−N_{CN} 91(1), N_{cyclam}−Ni−N_{cyclam} 85.5(2), 94.5(7), N_{CN}−Ni−O 177.4, N_{cyclam}−Ni−O 89(3). (Middle and lower) Portions of the one-dimensional $[(Me_3tacn)(cyclam)NiMo(CN)_3]^{2+}$ chains in the structures of **14** (middle) and **15** (lower). H atoms are omitted for clarity. Black, crosshatched, shaded, and white spheres represent Mo, Ni, C, and N atoms, respectively. In the lower structure, crystallographic inversion centers are located at the Ni atoms running along the middle of the chain.

consisting of a linear $[(Me_3tacn)_2(cyclam)NiMo_2(CN)_6]^{2+}$ unit capped on either end by a $[(cyclam)Ni(H_2O)]^{2+}$ moiety. With a minimum C−Mo···Mo−C torsion angle of 92.3°, the central linear unit has a conformation similar to that of the α isomer in **8**·2DMF (Figure 5, upper). A comparison of metric parameters (see Figure 9 legend and Table 3), however, shows the zigzag cluster to have a more linear bridging arrangement. No hydrogen bonding contacts directly between clusters are evident in the crystal structure.

To probe the magnetic properties of the zigzag cluster, measurements were carried out on a sample containing **13** together with precisely 7.13 equiv of $[(cyclam)NiBr_2]$. Results obtained from independent measurements of pure $[(cyclam)NiBr_2]$ under identical conditions were then subtracted to extract just that component of the data arising from **13**. The magnetization data indicate the presence of zero-field splitting; however, attempts at generating a fit were complicated by the apparent population of low-lying excited states. The magnetic susceptibility data (see Figure 10) are indeed consistent with a reduction in the strength of the exchange coupling relative to that observed in **8**−**10**. At room temperature, the value of $\chi_M T$ lies slightly below the spin-only value of 6.75 cm^3 K/mol expected for three $S = 1$ and two $S = 3/2$ ions with $g = 2.00$. As the temperature is lowered, $\chi_M T$ increases monotonically, until reaching a maximum of 14.11 cm^3 K/mol at 9 K. This behavior is consistent with the presence of ferromagnetic coupling to give an $S = 6$ ground state, which is further supported by the high-field magnetization data. When assuming that the strength of the magnetic coupling between each cyanide-bridged Mo^{III}−Ni^{II} pair is identical, attempts to simulate the susceptibility data failed to yield satisfactory results. Consequently, a model employing two different coupling constants—one for coupling with the central Ni atom and the other for coupling with either of the two outermost Ni atoms—was adopted with use of the following exchange Hamiltonian.

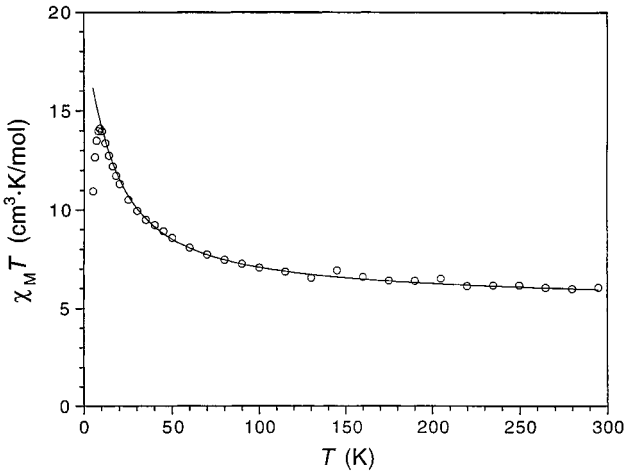

Figure 10. Magnetic behavior of $[(Me_3tacn)_2(cyclam)_3(H_2O)_2Ni_3Mo_2(CN)_6]Br_6$·$9H_2O$ (**13**), as measured at 1000 G. The solid line represents the calculated fit to the data.

$$\hat{H} = -2\{J[\hat{S}_{Ni(1)}\cdot(\hat{S}_{Mo(1)} + \hat{S}_{Mo(2)})] + J'(\hat{S}_{Ni(2)}\cdot\hat{S}_{Mo(1)} + \hat{S}_{Ni(3)}\cdot\hat{S}_{Mo(2)})\} \quad (9)$$

As shown in Figure 10, reasonable agreement with the higher temperature data is obtained with $J = 4.0$ cm^{-1}, $J' = 8.5$ cm^{-1}, and $g = 1.83$. Hence, it appears that attaching two Ni^{II} centers to the $[(Me_3tacn)Mo(CN)_3]$ unit can cause a substantial reduction in the strength of the magnetic exchange coupling. Although the magnitude of the reduction observed in this case is rather surprising, such a trend might be expected since coordination of a metal at the nitrogen end of a second cyanide ligand affects the molybdenum-based orbital that ultimately participates in both superexchange pathways. In addition, we note that the smaller coupling constant is associated with the central Ni^{II} ion, which is involved in exchange interactions with two Mo^{III} centers, rather than just one.

$NiMo(CN)_3$ Chains. Reactions related to eqs 5 and 8 above, but employing an equimolar ratio of reactants, generate com-

Table 4. Selected Mean Interatomic Distances (Å) and Angles (deg) for the One-Dimensional Chains in the Structures of $[(Me_3tacn)(cyclam)NiMo(CN)_3]I_2 \cdot 4H_2O$ (**14**) and $[(Me_3tacn)(cyclam)NiMo(CN)_3](ClO_4)_2 \cdot 1.5H_2O$ (**15**)[a]

	14	**15**
Mo−C	2.14(2)	2.09(8)
Ni−N_{CN}	2.12(1)	2.12(3)
C−N_{CN}	1.16(1)	1.18(2)
Mo−N_{tacn}	2.227(5)	2.24(1)
Ni−N_{cyclam}	2.06(1)	2.07(2)
C−Mo−C	89(3)	91(2)
Mo−C−N_{CN}	173(1)	173(4)
N_{CN}−Ni−N_{CN}	178.1(3)	179(2)
Ni−N_{CN}−C	171.6(2)	172(3)
N_{tacn}−Mo−C	95(3)	94(2)
	172.4(2)	171(2)
N_{tacn}−Mo−N_{tacn}	79.8(3)	79.4(4)
N_{cyclam}−Ni−N_{CN}	90(1)	90(1)
N_{cyclam}−Ni−N_{cyclam}	85.75(7)	85.1(2)
	94.3(9)	94.9(5)

[a] N_{CN}, N_{tacn}, and N_{cyclam} indicate N atoms in cyanide and Me_3tacn, and cyclam ligands, respectively.

pounds containing one-dimensional $[(Me_3tacn)(cyclam)NiMo(CN)_3]^{2+}$ chains.

$$[(Me_3tacn)Mo(CN)_3] + [(cyclam)Ni(H_2O)_2]^{2+} \rightarrow [(Me_3tacn)(cyclam)NiMo(CN)_3]^{2+} \quad (10)$$

Using iodide as the counterion leads to formation of $[(Me_3tacn)(cyclam)NiMo(CN)_3]I_2 \cdot 4H_2O$ (**14**), featuring the zigzag chain displayed in the middle of Figure 9. The structure is a simple extension of the zigzag cluster shown at the top of Figure 9, with every nickel cyclam complex coordinated axially by two $[(Me_3tacn)Mo(CN)_3]$ units. Accordingly, as listed in Table 4, its mean interatomic distances and angles are in close agreement with those observed in the structure of $\mathbf{13} \cdot 5H_2O$ (see Figure 9 legend). Carrying out reaction 10 with perchlorate as the counterion in place of iodide produces $[(Me_3tacn)(cyclam)NiMo(CN)_3](ClO_4)_2 \cdot 1.5H_2O$ (**15**), containing an isomeric chain with the more sinuous structure depicted at the bottom of Figure 9. The essential difference between the two chains is subtle, lying only in the direction of propagation at every fourth molybdenum center; as compared in Table 4, they possess very similar metric parameters. Thus, as for linear $[(Me_3tacn)_2(cyclam)NiMo_2(CN)_6]^{2+}$ cluster conformations, the chain structure adopted appears to be highly sensitive to the packing influences of the counterions and solvate molecules. Indeed, although all of the linear $NiMo_2(CN)_6$ segments in **14** have the α isomer conformation, the analogous segments in **15** alternate between α and β conformations. The latter structure in particular suggests that, with the right choice of counterion, a cyclized chain consisting of a discrete $[(Me_3tacn)_4(cyclam)_4Ni_4Mo_4(CN)_{12}]^{8+}$ square with all edges in a β conformation might be produced. Note, however, that none of the structures containing $[(Me_3tacn)Mo(CN)_3]$ complexes connected through nickel cyclam units exhibit Me_3tacn ligands in the fully eclipsed orientation required for an edge-bridged cubic cluster.

As might be expected, **14** and **15** display similar magnetic properties. Figure 11 shows the variation of $\chi_M T$ with temperature for **15**. At room temperature, it lies slightly above the spin-only value of 2.875 cm^3 K/mol expected for noninteracting $S = 1$ and $S = 3/2$ ions with $g = 2.00$. Consistent with

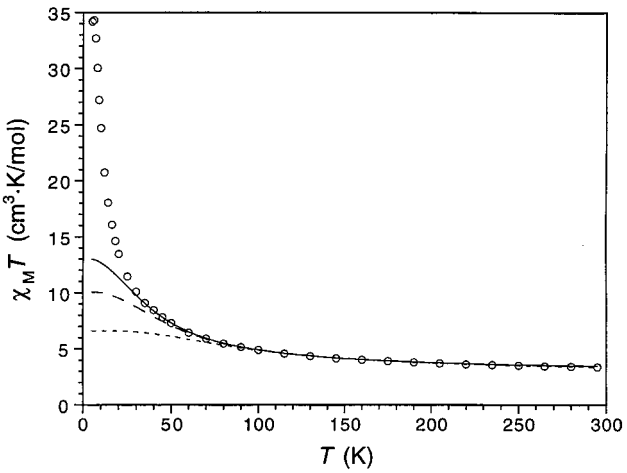

Figure 11. Magnetic behavior of the one-dimensional chain compound $[(Me_3tacn)(cyclam)NiMo(CN)_3](ClO_4)_2 \cdot 1.5H_2O$ (**15**), as measured at 1000 G. Simulations are shown for hypothetical, cyclic $[(Me_3tacn)(cyclam)NiMo(CN)_3]_n^{2n+}$ species with $n = 2$ (short dashes), 3 (long dashes), and 4 (solid line).

ferromagnetic coupling, $\chi_M T$ rises monotonically as the temperature decreases, until achieving a maximum of 34.33 cm^3 K/mol at 6 K. Attempts to simulate these data employed the usual approach of calculating the behavior for a sequence of cyclic oligomers of increasing size.[34] Calculations were performed for cyclic $[(Me_3tacn)(cyclam)NiMo(CN)_3]_n^{2n+}$ specieswith $n = 2-4$, using an exchange Hamiltonian of the following form.

$$\hat{H} = -2J[\hat{S}_{Ni(1)} \cdot (\hat{S}_{Mo(1)} + \hat{S}_{Mo(n)}) + \sum_{i=2}^{n} \hat{S}_{Ni(i)} \cdot (\hat{S}_{Mo(i-1)} + \hat{S}_{Mo(i)})] \quad (11)$$

For the larger cycles, the best agreement with the higher temperature data was obtained with $g = 1.95$ and $J = 13.1$ cm^{-1}, suggesting similar parameters for the infinite chain. The corresponding results from simulations of the data for **14** gave $g = 1.96$ and $J = 14.9$ cm^{-1}.[35] Here again, attaching two Ni^{II} centers to the $[(Me_3tacn)Mo(CN)_3]$ unit appears to cause a reduction in the strength of the magnetic exchange coupling, albeit to a much lesser extent than observed in **13**.

Outlook

The foregoing results demonstrate the feasibility of replacing Cr^{III} with Mo^{III} as a means of increasing both the strength of the magnetic exchange coupling and the magnetic anisotropy in a metal−cyanide cluster. This type of substitution can likely be extended to the many other cyanide-bridged clusters and solids containing magnetically coupled Cr^{III} centers. Indeed, $[(Me_3tacn)Mo(CN)_3]$ has already been shown to replace the $[(Me_3tacn)Cr(CN)_3]$ units in the trigonal prismatic cluster $[(Me_3tacn)_6MnCr_6(CN)_{18}]^{2+}$ possessing an $S = 13/2$ ground state.[5d,37] Similar replacements involving W^{III} or Re^{IV} instead of Mo^{III} are expected to further increase the exchange coupling and anisotropy. The possibility of incorporating these and other paramagnetic ions of second- and third-row transition-metals into metal−cyanide clusters with a high-spin ground state is currently under investigation. Ultimately, it is hoped that such

(37) Hee, A. G.; Sokol, J. J.; Long, J. R. Work in progress.

an approach will lead to new single-molecule magnets capable of storing data at more practical temperatures.

Acknowledgment. This research was funded by NSF Grant No. CHE-0072691, the Camille and Henry Dreyfus Foundation, the Alfred P. Sloan Foundation, the Hellman Family Faculty Fund, and the University of California, Berkeley. We thank NSF for providing J.J.S. with a predoctoral fellowship, Elf-Atochem for partial support of M.P.S., Dr. C. Crawford and Unilever for a donation of Me_3tacn, Profs. E. Coronado and D. N. Hendrickson for supplying software used to simulate magnetic data, Profs. J. K. McCusker and D. Gatteschi for helpful discussions, Profs. A. M. Stacy and A. Zettl for use of the SQUID magnetometers, and Prof. J. Arnold for use of the thermogravimetric analysis instrument.

Supporting Information Available: Cyclic voltammogram of **2** in DMF. Plots and fits of the magnetization data for **9** and **10** and of the magnetic susceptibility data for **6**, **9**, **10**, and **14**. X-ray structural information for **2**−**15**, including tables of crystal and refinement data, atomic positional and thermal parameters, and interatomic distances and angles (PDF). An X-ray crystallographic file (CIF). This material is available free of charge via the Internet at http://pubs.acs.org.

JA011645H